

Heat Transfer and Production in Cratonic Continental Crust: U-Pb Thermochronology of Xenoliths From the Siberian Craton

Francisco E Apen, Roberta L Rudnick, Dmitri A Ionov, John M Cottle, Jean-François Moyen, Alexander V Golovin, Andrey V Korsakov

▶ **To cite this version:**

Francisco E Apen, Roberta L Rudnick, Dmitri A Ionov, John M Cottle, Jean-François Moyen, et al.. Heat Transfer and Production in Cratonic Continental Crust: U-Pb Thermochronology of Xenoliths From the Siberian Craton. Geochemistry, Geophysics, Geosystems, 2022, 23 (10), 10.1029/2022GC010497 . hal-03823786

HAL Id: hal-03823786
https://uca.hal.science/hal-03823786

Submitted on 21 Oct 2022

HAL is a multi-disciplinary open access archive for the deposit and dissemination of scientific research documents, whether they are published or not. The documents may come from teaching and research institutions in France or abroad, or from public or private research centers.

L'archive ouverte pluridisciplinaire **HAL**, est destinée au dépôt et à la diffusion de documents scientifiques de niveau recherche, publiés ou non, émanant des établissements d'enseignement et de recherche français ou étrangers, des laboratoires publics ou privés.



Distributed under a Creative Commons Attribution - NonCommercial - NoDerivatives 4.0 International License

Check for updates

Geochemistry, Geophysics, Geosystems®

AGU ADVANCING EARTH AND SPACE SCIENCE

RESEARCH ARTICLE
10.1029/2022GC010497

Heat Transfer and Production in Cratonic Continental Crust: U-Pb Thermochronology of Xenoliths From the Siberian Craton

Francisco E. Apen[1], Roberta L. Rudnick[1], Dmitri A. Ionov[2], John M. Cottle[1], Jean-François Moyen[3], Alexander V. Golovin[4,5], and Andrey V. Korsakov[4]

[1]Department of Earth Science and Earth Research Institute, University of California, Santa Barbara, Santa Barbara, CA, USA, [2]Géosciences Montpellier, Université de Montpellier, Montpellier, France, [3]Université Jean-Monnet, Laboratoire Magmas et Volcans, UCA-CNRS-IRD, Aubière, France, [4]Sobolev Institute of Geology and Mineralogy, Siberian Branch, Russian Academy of Sciences, Novosibirsk, Russia, [5]Institute of the Earth's Crust, Siberian Branch, Russian Academy of Sciences, Novosibirsk, Russia

Key Points:

- The U-Pb system in deep crustal xenoliths is sensitive to transient heating of the lower crust and not just slow cooling
- The central Siberian craton lower crust resided below the Pb closure temperature of rutile and apatite prior to kimberlite eruption 360 Ma
- Extremely low crustal heat production for the craton (~0.3 μW/m^3) is consistent with peridotite xenolith *P-T* data

Supporting Information:

Supporting Information may be found in the online version of this article.

Correspondence to:

F. E. Apen,
apen@ucsb.edu

Citation:

Apen, F. E., Rudnick, R. L., Ionov, D. A., Cottle, J. M., Moyen, J.-F., Golovin, A. V., & Korsakov, A. V. (2022). Heat transfer and production in cratonic continental crust: U-Pb thermochronology of xenoliths from the Siberian craton. *Geochemistry, Geophysics, Geosystems*, *23*, e2022GC010497. https://doi.org/10.1029/2022GC010497

Received 29 APR 2022
Accepted 8 SEP 2022

Author Contributions:

Conceptualization: Roberta L. Rudnick
Formal analysis: Francisco E. Apen
Funding acquisition: Roberta L. Rudnick
Investigation: Francisco E. Apen
Methodology: Francisco E. Apen, John M. Cottle
Resources: Dmitri A. Ionov, John M. Cottle, Alexander V. Golovin, Andrey V. Korsakov
Supervision: Roberta L. Rudnick, John M. Cottle

© 2022. The Authors.
This is an open access article under the terms of the Creative Commons Attribution License, which permits use, distribution and reproduction in any medium, provided the original work is properly cited.

Abstract Coupled U-Pb and trace-element analyses of accessory phases in crustal xenoliths from the Late Devonian Udachnaya kimberlite (Siberian craton, Russia) are used to constrain Moho temperature and crustal heat production at the time of kimberlite eruption. Rutile and apatite in lower-crustal garnet granulites record U-Pb dates that extend from 1.8 Ga to 360 Ma (timing of kimberlite eruption). This contrasts with upper-crustal tonalites and amphibolites that contain solely Paleoproterozoic apatite. Depth profiling of rutile from the lower-crustal xenoliths show that U-Pb dates increase gradually from rim to core over μm-scale distances, with slower-diffusing elements (e.g., Al) increasing in concentration across similar length-scales. The U-Pb and trace element gradients in rutile are incompatible with partial Pb loss during slow cooling, but are consistent with neocrystallization and re-heating of the lower crust for <1 Myr prior to eruption. Because Paleoproterozoic rutile and apatite dates are preserved, we infer that long-term ambient lower-crustal temperatures before this thermal perturbation were cooler than the Pb closure temperature of rutile and probably apatite (<400°C). The lower-crustal temperature bounds from these data are consistent with pressure-temperature arrays of Udachnaya peridotite xenoliths that suggest relatively cool geothermal gradients, signifying that the mantle xenoliths accurately capture the thermal state of the lithosphere prior to eruption. Combined, the xenolith data imply low crustal heat production for the Siberian craton (~0.3 μW/m^3). Nevertheless, such values produce surface heat flow values of 20–40 mW/m^2, higher than measured around Udachnaya (average 19 mW/m^2), suggesting that the surface heat flow measurements are inaccurate.

Plain Language Summary The decay of radioactive elements, like uranium (U), thorium (Th), and potassium (K), produces heat and the dissipation of this heat from Earth's interior drives flow at depth and the movement of tectonic plates at the surface over geologic time. The crust—the planet's rocky outer layer—is hypothesized to contain a significant portion of Earth's heat-producing elements, yet this budget is uncertain. The total amount of heat leaving the surface can be measured, but how much of this flux reflects heat production within the crust versus heat derived from the underlying mantle is also uncertain. Kimberlite pipes carry fragments of Earth's interior to the surface ("xenoliths") in Siberia. Some of the xenoliths are from near the base of the crust, and temperature-sensitive chronometers in these rocks record ancient dates (>1 billion years old). Such ancient dates are significant because they can only be preserved if temperatures in the deep crust were cool (<400°C). Models of heat transfer through the Siberian crust using our results and mantle xenolith pressure-temperature data indicate relatively low heat production in the crust.

1. Introduction

Temperatures of the lower crust and Moho are important boundary conditions for models of heat transfer and production in the lithosphere as well as models of the bulk composition of the continental crust (e.g., Hacker et al., 2015; Jaupart & Mareschal, 2014; R. L. Rudnick et al., 1998; Sandiford & McLaren, 2002). Surface heat flow measurements reveal the total amount of heat exiting the lithosphere (a combination of mantle heat flow entering the base of the lithosphere and heat produced within the crust and lithospheric mantle by the decay of radioactive elements), yet temperatures near the Moho are poorly constrained, making it difficult to unravel the respective contributions of the mantle and crust to the total heat budget of the lithosphere. Seismic wavespeeds

15252027, 2022, 10, Downloaded from https://agupubs.onlinelibrary.wiley.com/doi/10.1029/2022GC010497 by Cochrane France, Wiley Online Library on [21/10/2022]. See the Terms and Conditions (https://onlinelibrary.wiley.com/terms-and-conditions) on Wiley Online Library for rules of use; OA articles are governed by the applicable Creative Commons License

Validation: Roberta L. Rudnick, Dmitri A. Ionov, John M. Cottle, Jean-François Moyen, Alexander V. Golovin, Andrey V. Korsakov
Visualization: Francisco E. Apen
Writing – original draft: Francisco E. Apen
Writing – review & editing: Roberta L. Rudnick, Dmitri A. Ionov, John M. Cottle, Jean-François Moyen, Alexander V. Golovin, Andrey V. Korsakov

and other geophysical observations (magnetic Curie depth estimates, electrical conductivity, Pn velocity, etc.; Goes et al., 2020) provide snapshots of the thermal profile of the crust whereas xenoliths—fragments derived from in situ lower crust transported rapidly to the surface by volcanism—yield direct insights into long-term thermal histories (e.g., Hasterok & Chapman, 2011; R. L. Rudnick et al., 1998).

Thermobarometry of xenoliths can, in principle, be used to establish temperature and pressure conditions within the lithosphere. However, a long recognized problem with this approach—most notably in stable cratonic regions—is that different lithologies record distinct geothermal gradients (e.g., Semprich & Simon, 2014). Pressure-temperature (*P*-*T*) arrays for cratonic mantle xenoliths define relatively cool geothermal gradients through the lithosphere (30–45 mW/m^2 geotherms) and projections of these gradients to the Moho suggests temperatures of 400°C–600°C (Garber et al., 2018; Hasterok & Chapman, 2011; R. L. R. Rudnick & Nyblade, 1999). Mantle xenoliths, however, only provide indirect constraints on Moho temperatures because robust thermobarometric calibrations are restricted to lithologies that equilibrated relatively deep within the lithosphere in the garnet stability field (e.g., Brey & Köhler, 1990). Garnet granulite xenoliths could provide direct constraints on the thermal state of the lower crust, yet thermobarometry of such xenoliths suggests geothermal gradients higher than for peridotite xenoliths from the same pipes (e.g., >60 mW/m^2; Jones et al., 1983; Semprich & Simon, 2014). This issue arises because most granulite xenoliths are refractory and anhydrous, and thus fail to re-equilibrate following peak metamorphic conditions (e.g., Frost & Chacko, 1989; Pattison, 2003; Pattison & Bégin, 1994).

The U-Pb isotope system holds much promise for extracting long-term thermal histories of the deep crust from xenoliths (Apen et al., 2020; Davis, 1997; Davis et al., 2003; Edwards & Blackburn, 2018; O'Sullivan et al., 2021; Schmitz & Bowring, 2003; T. Blackburn et al., 2011; T. J. Blackburn et al., 2012). U-Pb thermochronology exploits both the radioactive decay of U to Pb and the temperature-dependent diffusivity of Pb in different minerals. The U-Pb dates of common accessory phases in crustal rocks (e.g., zircon, rutile, and apatite) reflect the different degrees of Pb diffusion as a function of temperature and time (e.g., Schmitz & Bowring, 2003; Smye et al., 2018; T. Blackburn et al., 2011). For zircon, significant diffusion of Pb occurs at >1000°C, for rutile >500°C–600°C, and apatite >350°C–450°C (all assuming a 50–500-μm-radius sphere and 0.01°C–0.1°C/Myr cooling rates; Cherniak, 2010; Smye et al., 2018). In the case of xenoliths, these phases are expected to experience different degrees of Pb diffusion during their tenure in the deep crust before being entrained in the host magma and carried to the surface (Schmitz & Bowring, 2003; T. Blackburn et al., 2011). For example, if a xenolith resided at 500°C for 100 Myr, Pb diffusion in zircon and rutile is insignificant and the U-Pb system should exhibit closed-system behavior such that dates older than magmatic entrainment can be retained in these phases. At the same conditions, Pb diffusion in apatite would be significant (open-system behavior), resulting in U-Pb dates that overlap the timing of eruption, reflecting rapid cooling upon eruption.

A tenet in developing thermal models for the lower crust based on U-Pb thermochronology is the notion that Pb undergoes thermally mediated volume diffusion at ambient lower-crustal temperatures. Indeed, xenolith transport in kimberlites and alkali basalts is too rapid (on the order of hours to days; Spera, 1984) to significantly disturb the U-Pb system in most accessory phases (Schmitz & Bowring, 2003). Xenoliths, however, may be heated during episodes of advective magmatic heating or fluid flow prior to their entrainment, and such heating could induce partial Pb loss in thermochronometers (e.g., Apen et al., 2020; Hacker et al., 2000; Jollands et al., 2018; Smit et al., 2016). Any inferences on lithospheric thermal structure based on xenoliths and their mineral constituents must therefore delineate primary signatures of crustal relaxation (on the order of 100–1,000 Myrs) from shorter-term heating by magmatic intrusion or metasomatism (<1 Myr). Spatially resolved analysis of multiple trace elements with different diffusivities can discriminate signatures of long-term cooling from shorter-term heating events in the lower crust: diffusive length scales should vary according to diffusivities, with faster diffusing elements showing more pronounced length scales of diffusion than slower diffusing ones (Apen et al., 2020; Garber et al., 2020; Holder et al., 2019; Stearns et al., 2016).

To test the fidelity of U-Pb thermochronology as a tool for constraining the long-term thermal history of the deep crust, we have undertaken laser ablation split stream (LASS) U-Pb and trace-element analyses of accessory phases in crustal xenoliths from the Udachnaya kimberlite located within the central Siberian craton (Figure 1). The xenolith suite covers a broad range of lithologies, including granitoids, amphibolites, and garnet-bearing granulites. This lithological diversity is interpreted as sampling different levels of the crustal column at Udachnaya. The new laser ablation data, combined with new thermobarometry and pseudosection modeling, are used to

15252027, 2022, 10, Downloaded from https://agupubs.onlinelibrary.wiley.com/doi/10.1029/2022GC010497 by Cochrane France, Wiley Online Library on [21/10/2022]. See the Terms and Conditions (https://onlinelibrary.wiley.com/terms-and-conditions) on Wiley Online Library for rules of use; OA articles are governed by the applicable Creative Commons License

15252027, 2022, 10, Downloaded from https://agupubs.onlinelibrary.wiley.com/doi/10.1029/2022GC010497 by Cochrane France, Wiley Online Library on [21/10/2022]. See the Terms and Conditions (https://onlinelibrary.wiley.com/terms-and-conditions) on Wiley Online Library for rules of use; OA articles are governed by the applicable Creative Commons License

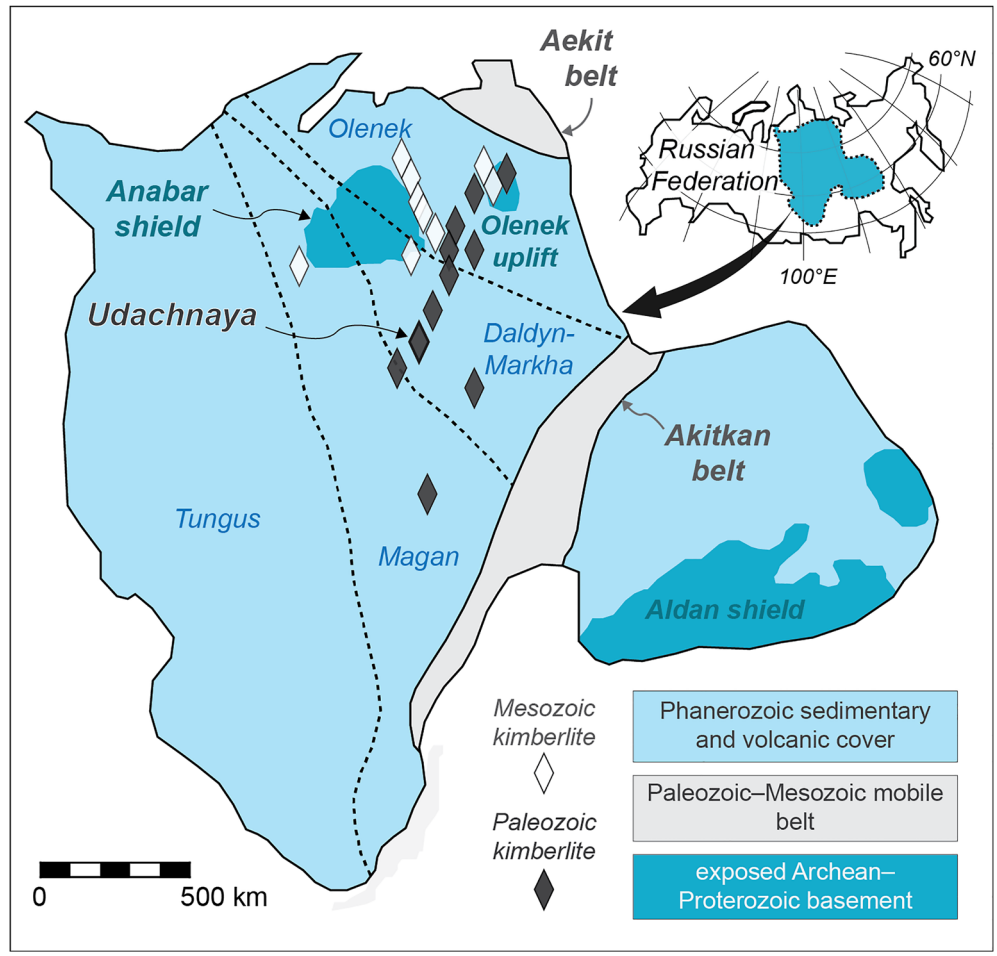


Figure 1. Simplified geologic map of the Siberian craton (after Moyen et al., 2017). Dashed lines delineate the boundaries of different blocks that make up the craton. Diamonds denote the location of kimberlites, with white diamonds corresponding to Mesozoic kimberlites and gray diamonds showing Paleozoic kimberlites.

probe the thermal state of the crust prior to eruption and develop models of heat transfer and production within the Siberian craton.

2. Geologic Background and Previous Xenolith Work

Most of the Siberian craton is overlain by thick Phanerozoic sedimentary and volcanic cover (Cherepanova et al., 2013), but information about crust formation and structure is gleaned from limited basement outcrops and kimberlite-hosted xenoliths (Figure 1). Based on geophysical data and outcrops in the Anabar shield, the craton is divided into five major terranes: Tungus, Magan, Daldyn-Markha, Olenek, and Aldan (see summaries in Rosen, 2002). Basement gneisses and granulites exposed in the Anabar shield reveal that the central craton is composed of Archean crust (ca. 3.6–2.7 Ga) reworked throughout the Archean and Proterozoic as well as juvenile Proterozoic crust (2.1–1.8 Ga) (Figure 1; Moyen et al., 2017; Paquette et al., 2017; Rosen, 1989; Smelov et al., 2012). Collision of the Tungus, Magan, Daldyn-Markha, and Olenek terranes to form the Siberian craton occurred 2.1–1.8 Ga based on the geochronology and geochemistry of Paleoproterozoic granitoids and metamorphic rocks of the Anabar shield (Rosen, 2002; Rosen et al., 2006). Re-Os dating of peridotite xenoliths yields similar age intervals for the formation and reworking of the underlying cratonic lithospheric mantle (Ionov et al., 2020; Moyen et al., 2017).

Kimberlites abound in the central and northern parts of the craton (Figure 1). Most kimberlites were emplaced in the Paleozoic (450–340 Ma) and Mesozoic (250–130 Ma) (Kinny et al., 1995; Sun et al., 2014) and are rich

15252027, 2022, 10, Downloaded from https://agupubs.onlinelibrary.wiley.com/doi/10.1029/2022GC010497 by Cochrane France, Wiley Online Library on [21/10/2022]. See the Terms and Conditions (https://onlinelibrary.wiley.com/terms-and-conditions) on Wiley Online Library for rules of use; OA articles are governed by the applicable Creative Commons License

sources of xenoliths/xenocrysts that provide information on the age and structure of the craton where it is otherwise concealed (e.g., Ionov et al., 2010; Kostrovitsky et al., 2016; M. Koreshkova et al., 2009; Moyen et al., 2017). The diamondiferous Udachnaya kimberlite pipe erupted through the Daldyn-Markha terrane ca. 360 Ma (U-Pb perovskite; Kinny et al., 1995; Sun et al., 2014) and hosts an extensive suite of mantle and crustal xenoliths. Thermobarometry of Udachnaya garnet peridotite xenoliths suggests that the lithosphere is thick (>200 km) and cold (Agashev et al., 2013; Boyd, 1984; Doucet et al., 2012; Goncharov et al., 2012; Ionov et al., 2010, 2015, 2020; Liu et al., 2022). Radiogenic isotopes in harzburgite xenoliths (Re-Os, Lu-Hf, and Sm-Nd) suggest a dominantly Proterozoic age for the lithosphere mantle (2.2–1.8 Ga; Doucet et al., 2014; Ionov et al., 2015, 2020), but dunites, eclogites, and olivine megacrysts also indicate Archean ages (Re-Os and Sm-Nd model ages up to 3.2 Ga; Ionov et al., 2020; Pearson et al., 1995). Re-Os model ages as young as 360 Ma are also present and have been interpreted to reflect Re addition during kimberlite emplacement (Ionov et al., 2015, 2020).

Crustal xenoliths from Udachnaya include granitoids, amphibolites, mafic garnet granulites, and felsic garnet granulites, some of which are probably sedimentary in origin (e.g., Jin et al., 2021; M. Koreshkova et al., 2009; Moyen et al., 2017; M. Y. Koreshkova et al., 2011; V. S. Shatsky et al., 2016, 2019). Zircon U-Pb dates from lower-crustal granulite xenoliths are dominantly Paleoproterozoic—ranging between 1.9 and 1.8 Ga—though some granulite xenoliths contain zircon with Archean inheritance (2.8–2.7 Ga) (M. Koreshkova et al., 2009; Moyen et al., 2017; Rosen, 2002; Rosen et al., 2006; V. S. Shatsky et al., 2016, 2019). This contrasts with shallower granitoid and amphibolite xenoliths that contain Archean zircon with no concordant Paleoproterozoic dates (Moyen et al., 2017). Net-transfer reaction and cation exchange thermobarometry of garnet granulite xenoliths indicate equilibration at 0.6–1.2 GPa and 800°C–900°C (Jin et al., 2021; M. Y. Koreshkova et al., 2011). Significant 100°C–200°C cooling is also recorded by Fe-Mg temperatures from garnet and pyroxene rims and by the presence of retrograde amphibole in some granulite xenoliths (Jin et al., 2021; M. Y. Koreshkova et al., 2011).

The crust in the vicinity of Udachnaya is 44–46 km thick (Cherepanova et al., 2013; Mackey et al., 1998). Surface heat flow data across the Siberian craton are sparse, but the six measurements within ∼100 km of Udachnaya yield an average value of 19 ± 3 mW/m^2 (1SD) (Fuchs et al., 2021, and references therein). As it stands, these data are among the lowest surface heat flow values observed for any craton (cf., Jaupart et al., 2016). If accurate, they require either exceedingly low heat production in the crust, a low mantle heat flux, or both (Jaupart et al., 2016; R. L. Rudnick et al., 1998). Alternatively, the surface heat flow measurements may be inaccurate, possibly compromised by the thick sedimentary/volcanic cover overlying the crystalline basement around Udachnaya (Cherepanova et al., 2013), regional brine aquifers (Kitayama et al., 2017, and references therein), and/or Ice-Age glaciation (Birch, 1948; Jaupart & Mareschal, 2007). Low crustal heat production for the central Siberian craton is permissible based on regional magnetic Curie depths (580°C isotherm) estimated to be >35-km-deep (Gard & Hasterok, 2021).

3. Samples

The sample suite consists of 18 xenoliths analyzed and discussed by Moyen et al. (2017), as well as five new xenoliths. Petrographic descriptions with photomicrographs for the new samples are provided in Supporting Information S1. Rather than detailing the work done on all 23 samples (mostly U-Pb), we selected a subset of seven representative samples for in-depth investigation that are inferred to sample different levels of the crustal column at Udachnaya: two tonalites (samples 01-104 and 02-154), one amphibolite (sample 02-114), and four garnet granulites (samples 01-34, 79-14, 01-95, and 36-14) (Figure 2). Three of the latter (01-34, 79-14, and 01-95) are mafic garnet granulites composed of garnet + clinopyroxene + plagioclase ± orthopyroxene, and one (36-14) is a felsic garnet granulite composed of garnet + orthopyroxene + plagioclase + quartz + graphite.

All of the granulites exhibit granoblastic textures, and their mineral assemblages are well-preserved (Figure 2). The xenoliths are generally fresh, by comparison with many of those from previous work, though some of the granulites show textural evidence for minor alteration, like pockets of very-fine grained material interpreted to be former melt (e.g., mafic garnet granulite 79-14) and biotite clusters interpreted to have formed by re-hydration (e.g., mafic garnet granulite 01-95) (Figure 2). Rutile in garnet granulite xenoliths is typically 50–200 μm long and euhedral and occurs in the matrix—usually adjacent to garnet. Rutile is also found as inclusions within garnet and clinopyroxene (e.g., Figure 2c), indicating crystallization during peak granulite-facies metamorphism. Rutile appears free of ilmenite rims and exsolutions and does not contain obvious titanite or ilmenite overgrowths. Apatite grains are euhedral stubby prisms 50–200 μm long and 20–150 μm wide and are found both in

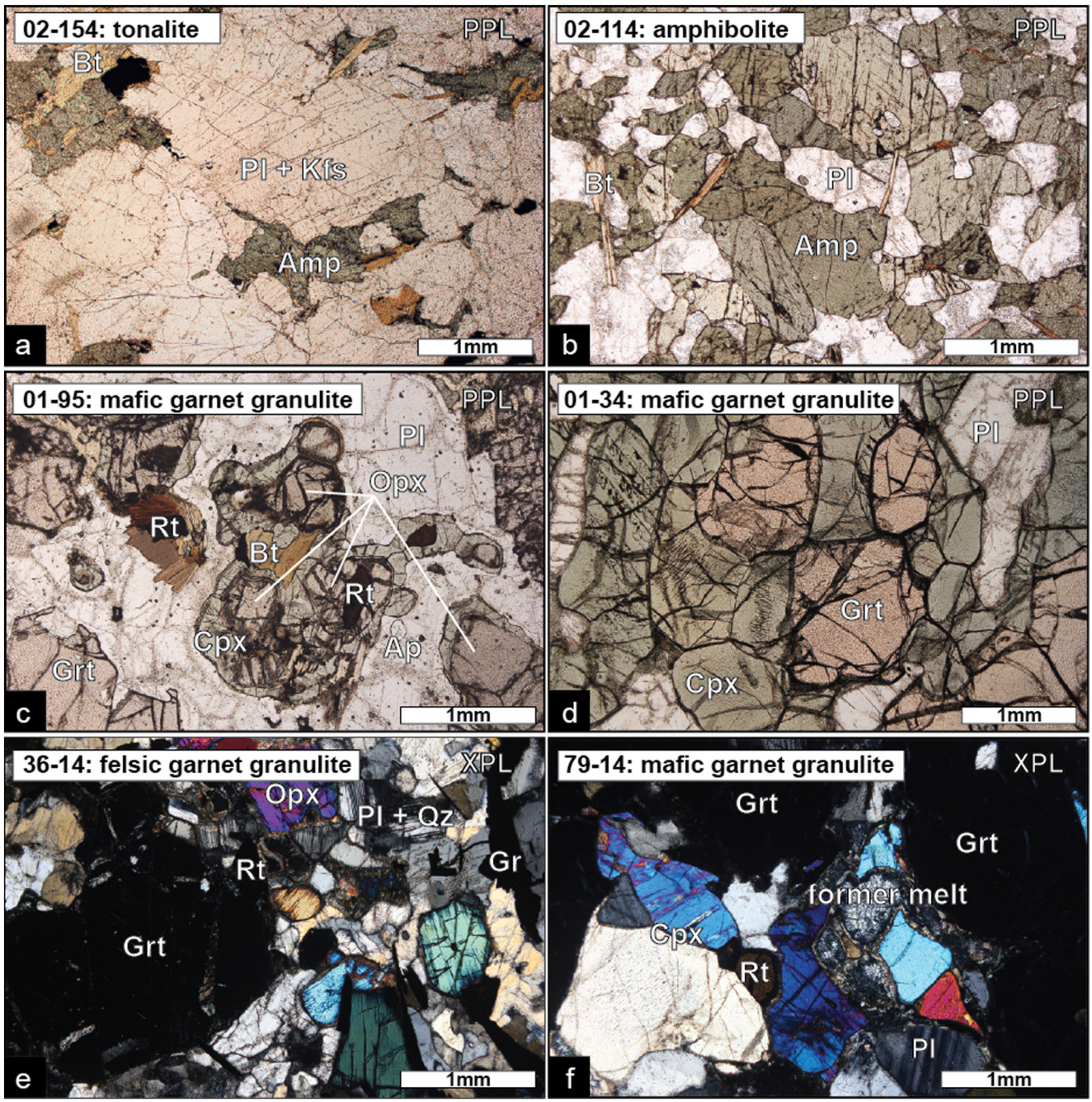


Figure 2. Representative photomicrographs of Udachnaya crustal xenoliths. (a) Tonalite xenolith 02-154. (b) Amphibolite xenolith 02-114. (c) Mafic garnet granulite 01-95. Note the orthopyroxene cores within clinopyroxene and biotite sourrounding rutile. (d) Mafic garnet granulite 01-34. (e) Felsic garnet granulite 36-14. (f) Mafic garnet granulite 79-14. Mineral abbreviations after Whitney and Evans (2010). PPL, plane polarized light; XPL, crossed polarized light.

the matrix and as inclusions in garnet. Notably, in mafic garnet granulites 01-95 and 79-14 apatite crystals contain thin exsolutions in their cores (Figure 2c).

We present results from thermobarometry and coupled U-Pb and trace-element analyses of accessory phases for the seven xenoliths. Zircon and apatite were analyzed for the tonalites and amphibolite (these rocks contain no other phases datable by U-Pb). Apatite and rutile were analyzed in all four of the granulites, whereas zircon was only found in two of them (01-95 and 36-14).

15252027, 2022, 10, Downloaded from https://agupubs.onlinelibrary.wiley.com/doi/10.1029/2022GC010497 by Cochrane France, Wiley Online Library on [21/10/2022]. See the Terms and Conditions (https://onlinelibrary.wiley.com/terms-and-conditions) on Wiley Online Library for rules of use; OA articles are governed by the applicable Creative Commons License

15252027, 2022, 10, Downloaded from https://agupubs.onlinelibrary.wiley.com/doi/10.1029/2022GC010497 by Cochrane France, Wiley Online Library on [21/10/2022]. See the Terms and Conditions (https://onlinelibrary.wiley.com/terms-and-conditions) on Wiley Online Library for rules of use; OA articles are governed by the applicable Creative Commons License

4. Analytical Methods

4.1. Electron Probe Microanalyses

Quantitative elemental analyses of major mineral phases were done using a Cameca SX-100 electron probe micro analyzer housed at the University of California, Santa Barbara. Measurements were made using the following beam conditions: an accelerating voltage of 20 kV, a beam current of 200 nA and a defocused beam of 2–5 μm diameter. A series of natural and synthetic standards were analyzed for calibration purposes.

4.2. Thermobarometry

Pressures and temperatures for the xenoliths were estimated using end-member equilibria among key minerals (mode 2 in THERMOCALC; Powell et al., 1998). Equilibration pressures and temperatures for the mafic garnet granulites were determined using garnet-clinopyroxene Fe-Mg exchange, garnet-clinopyroxene-plagioclase-quartz (GADS) equilibria, and albite-jadeite-quartz equilibria (AJQ; Brey & Köhler, 1990; Holland, 1980; Newton & Perkins, 1982; O'Brien & Rotzler, 2003); because no free quartz is present in the three mafic garnet granulites (01-95, 79-14, and 01-13), the calculated GADS and AJQ pressures represent maxima. Further, because we assumed no Fe^{3+} in the minerals, Fe-Mg exchange temperatures should also be considered maxima (Nimis et al., 2015). For felsic granulite 36-14, garnet-orthopyroxene Fe-Mg exchange thermometry and garnet-orthopyroxene-plagioclase-quartz (GAHS) constrain equilibration *P-T* (Newton & Perkins, 1982). These data were supplemented with single-mineral cation thermobarometry, including: Ca- and Al-in-orthopyroxene and Zr-in-rutile (Brey & Köhler, 1990; Tomkins et al., 2007). We utilized the amphibole-plagioclase barometer of Molina et al. (2015) for amphibolite 02-114 and the Al-in-amphibole barometer calibration of Anderson and Smith (1995) for tonalites 01-104 and 02-154; temperatures for both amphibolites and tonalites were calculated using the edenite-richterite thermometer of Holland and Blundy (1994).

We compared results from net-transfer and exchange reactions to pseudosection models developed using Perple_X (Connolly, 2009; Connolly & Kerrick, 1987). Models used the internally consistent thermodynamic data set of Holland and Powell (2011) and the metabasite set of solution models recommended by Green et al. (2016) and Palin et al. (2016). Whole-rock data used for pseudosection modeling are from Moyen et al. (2017); the whole-rock compositions of the newly analyzed xenoliths were determined using X-ray fluorescence at the Geoanalytical Lab at Washington State University. Details are reported in Supporting Information S1.

4.3. Laser Ablation Split-Stream Analyses

The xenoliths were processed using standard mineral separation techniques to recover whole grains (hand crushing, magnetic separation, and heavy liquid separation). Coupled U-Pb and trace element analyses on zircon, rutile, and apatite were done by LASS inductively coupled plasma mass spectrometry at UC Santa Barbara (Kylander-Clark, 2013, 2017). Analyses were conducted on polished grain interiors for conventional LASS analyses and on the unpolished exterior of whole grains for depth profiling. Analytical protocols are detailed in Supporting Information S1. The quoted uncertainties for all laser ablation data are 2σ and incorporate analytical uncertainty as well as additional uncertainties associated with reproducibility of secondary matrix-matched reference materials (Horstwood et al., 2016). Reported uncertainties for trace-element data are 2σ and only include analytical uncertainties. All U-Pb data are shown in Tera-Wasserburg concordia plots (Vermeesch, 2018) and are uncorrected for common-Pb. The quoted U-Pb dates for apatite and rutile are common-Pb corrected using a common-Pb intercept defined by a linear regression through the U-Pb data or assuming a Stacey and Kramers (1975) initial $^{207}Pb/^{206}Pb$ composition. The quoted dates for zircon are $^{207}Pb/^{206}Pb$ dates that are within 5% concordance of their respective $^{206}Pb/^{238}U$ date.

The sampling resolution of laser ablation spot analyses described above (50-μm-diameter spots for rutile) is too coarse to resolve age gradients. For this reason, depth profiling was done using continuous laser pulsing at a low frequency (e.g., Apen et al., 2020; Cottle et al., 2009; Garber et al., 2020; Holder et al., 2019; Smye & Stockli, 2014). Details regarding depth profiling are also reported in Supporting Information S1. Final pit depths were measured on the SEM and are on average ~13 μm. The depth profile data are reported at 1 s intervals and the reported U-Pb uncertainties take into account the reproducibility of multiple reference rutiles (~6% on $^{238}U/^{206}Pb$ and ~4% on $^{207}Pb/^{206}Pb$). In addition to U-Pb ratios, we also report Pb concentration profiles,

15252027, 2022, 10, Downloaded from https://agupubs.onlinelibrary.wiley.com/doi/10.1029/2022GC010497 by Cochrane France, Wiley Online Library on [21/10/2022]. See the Terms and Conditions (https://onlinelibrary.wiley.com/terms-and-conditions) on Wiley Online Library for rules of use; OA articles are governed by the applicable Creative Commons License

which we divided into radiogenic Pb (Pb*) and non-radiogenic (common) Pb (Pb_c) (see also Garber et al., 2020; Holder et al., 2019). The total concentrations of $^{207,206}Pb$ at each depth interval were calculated using the measured $^{238}U/^{206}Pb$ ratio, $^{207}Pb/^{206}Pb$ ratio, and U concentration and assuming an invariant $^{238}U/^{235}U$ ratio of 137.818 (Hiess et al., 2012). Concentrations of $^{207,206}Pb^*$ were determined using common-Pb corrected dates and measured U concentrations. From this, we calculated the proportion of Pb_c by subtracting $^{207,206}Pb^*$ from the total $^{207,206}Pb$ concentrations. The final $^{207,206}Pb^*$ profiles were further corrected for radiogenic Pb ingrowth following kimberlite eruption at 360 Ma.

4.4. Testing Thermal Histories With Depth Profiling

In order to quantify temperatures and timescales of diffusion using U, Pb, and other elements, we consider the inverse error functions of normalized elemental gradients (Crank, 1979), expressed as:

$$\mathrm{erf}^{-1}\left(\frac{C_x - C_r}{C_c - C_r}\right) = \left(\frac{x}{\sqrt{4 \times D(T) \times t}}\right)$$

where C_x is the concentration at a given position (x) within the grain, C_r is the concentration at the rim, C_c is the concentration at the core (or in this study, the bottom of the ablation pit), $D(T)$ is temperature-dependent diffusivity, and t is the time that the mineral spent at temperature T.

The length-scales of diffusion for elements in rutile are constrained by experiments. Diffusivities of Pb, Al, Si, Cr, Fe, Zr, Nb, Hf, and Ta in rutile vary by orders of magnitude, with relative diffusivities at a reference temperature of 700°C in the following order: $D_{Al} > D_{Si} > D_{Hf} \approx D_{Zr} > D_{Pb} > D_{Ta} \approx D_{Nb} > D_{Cr} > D_{Fe}$ (Cherniak, 2000; Cherniak & Watson, 2019; Cherniak et al., 2007; Marschall et al., 2013; Sasaki et al., 1985).

In addition to diffusion modeling, comparing U-Pb dates of different accessory phases aids in reconstructing thermal histories. Experimentally- and empirically derived Pb diffusion coefficients in rutile and apatite suggest that rutile has a higher Pb closure temperature than apatite (e.g., Smye et al., 2018). For simple linear cooling and similar grain sizes, one would then predict U-Pb dates from rutile to be exclusively older than apatite (Dodson, 1973). We discuss the thermal history of the Siberian craton lower crust within this framework.

5. Results

5.1. Thermobarometry and Pseudosection Modeling

The stability field of the observed garnet-clinopyroxene-plagioclase-rutile assemblage in the mafic garnet granulites (samples 01-95, 79-14, and 01-34) encompasses a large P-T range (1.0–1.6 GPa and 600°C–900°C). These estimates are consistent with the intersections of GADS, AJQ, and Fe-Mg garnet-pyroxene reactions determined using THERMOCALC (0.9–1.5 GPa and 750°C–900°C), despite the absence of quartz in the xenolith's main mineral assemblage. The presence of relict orthopyroxene (occurring exclusively as cores within clinopyroxene) in mafic garnet granulite 01-95 documents crystallization at slightly lower pressures; assuming relict orthopyroxene was in equilibrium with garnet, Ca-in-orthopyroxene thermometry suggests earlier metamorphism at 0.9 GPa and 825°C. Temperatures based on the composition of garnet and clinopyroxene rims indicate cooler temperatures of 630°C–710°C. Intersections of garnet isopleths in Perple_X did not produce results compatible with the P-T data from endmember equilibria (see Supporting Information S1 for further details); this could reflect contamination of the xenolith's whole rock compositions by the kimberlite and associated fluids (e.g., M. Y. Koreshkova et al., 2011) or limitations in the application of activity models (e.g., pyroxene; Forshaw et al., 2019). No whole-rock data exists for felsic granulite 36-14 so we rely on the positions and intersections of net-transfer and exchange reactions determined from THERMOCALC. The average P-T is 1.3 ± 0.4 GPa and 950°C ± 120°C; Fe-Mg temperatures from garnet and orthopyroxene rims are 700°C–750°C. Amphibole-plagioclase thermobarometry for both tonalites and amphibolites yields 0.3–0.5 GPa and 700°C–750°C.

5.2. U-Pb and Trace Element Data

Concordant zircon populations in tonalite xenoliths 01-104 and 02-154 and amphibolite xenolith 02-114 are Neoarchean (dominantly ca. 2.7 Ga with two younger dates at ca. 2.5 and 1.9 Ga in sample 02-154), consistent

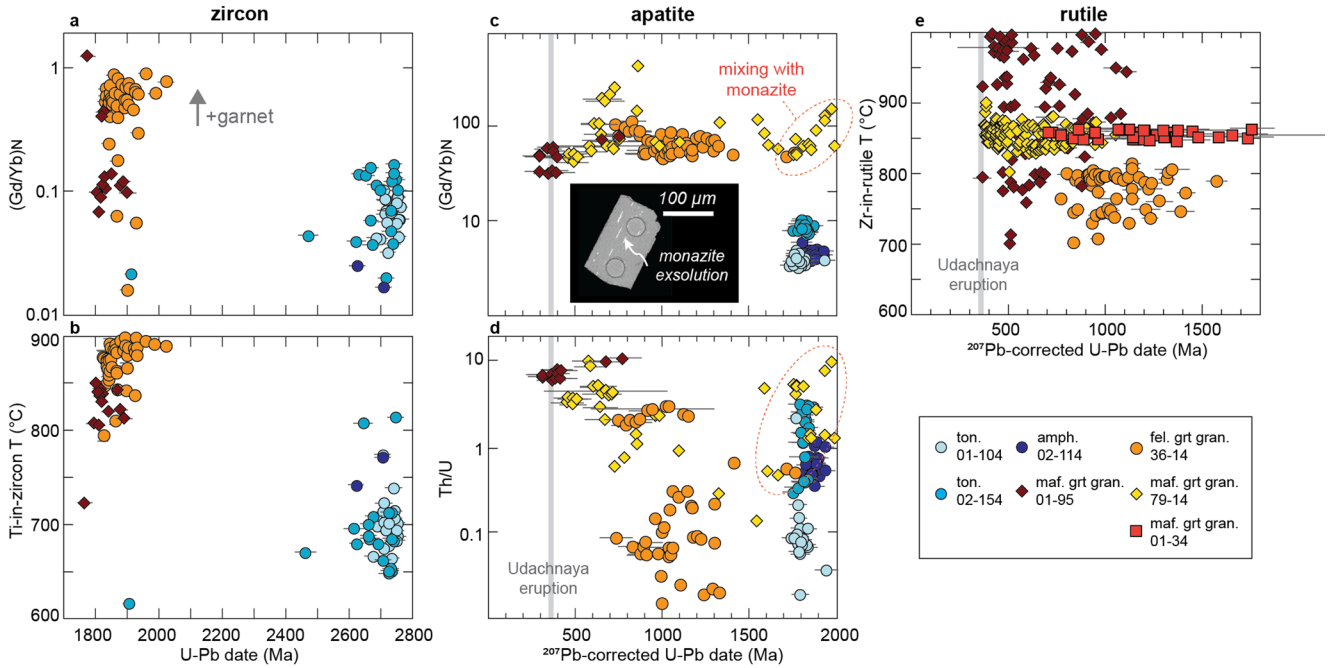


Figure 3. Summary of laser ablation split stream data. (a) Concordant zircon U-Pb dates versus $(Gd/Yb)_N$ (proxy for garnet growth) and Ti-in-zircon temperature (Ferry & Watson, 2007). Note that zircon from garnet granulites (01-95 and 36-14) show evidence for garnet-grade metamorphism at 1.9–1.8 Ga whereas zircon from tonalite and amphibolite xenoliths (01-104, 02-154, and 02-114) show crystallization at 2.7 Ga. Ti-in-zircon thermometry suggests metamorphism at 800°C–900°C for the garnet granulites and ~700°C crystallization of zircon in tonalite and amphibolite xenoliths. (b) Apatite common-Pb corrected U-Pb date versus $(Gd/Yb)_N$ and Th/U ratios. Apatite from tonalite and amphibolite xenoliths record 1.8–1.7 Ga dates whereas apatite from the garnet granulites record a large range of dates, including the eruption age of the Udachnaya kimberlite (represented by vertical gray bar). Inset: Apatite analyses with fine-scale monazite lamellae. Mixed apatite-monazite analyses are indicated by the dashed orange ellipse. (c) Rutile common-Pb corrected U-Pb date versus Zr-in-rutile temperatures. Note that although rutile U-Pb dates span a large age range, Zr temperatures generally show a limited range.

with findings of Moyen et al. (2017) (Figures 3a and 3b). Concordant Neoarchean zircon spot analyses have positively sloped heavy rare earth element (HREE) patterns as seen in low $(Gd/Yb)_N$ ratios (<0.2; Figure 3a), and Ti concentrations of 2–25 ppm, corresponding to temperatures of 610°C–830°C using the Ti-in-zircon thermometer calibration of Ferry and Watson (2007) (Figure 3b). Apatites in the same xenoliths yield Paleoproterozoic U-Pb dates (1.86–1.76 Ga) and are characterized by HREE-depleted REE patterns, expressed as $(Gd/Yb)_N$ ratios <10 (Figure 3c).

Zircon in garnet granulite xenoliths 01-95 and 36-14 yields Paleoproterozoic U-Pb dates in a similar 2.1–1.8 Ga age range (Figures 3a and 3b). Zircon in felsic granulite 36-14 has flat HREE patterns ($(Gd/Yb)_N$ ratios >0.1; Figure 3a), and Ti concentrations of 16–53 ppm, corresponding to temperatures of 840°C–930°C (Figure 3b). Zircon in mafic granulite 01-95 has mostly positively sloped HREEs ($(Gd/Yb)_N$ ratios ~0.1; Figure 3a) and Ti concentrations of 19–28 ppm or Ti-in-zircon temperatures in the range of 810°C–850°C (Figure 3b).

Only apatite from mafic garnet granulites 01-95 and 79-14 and felsic garnet granulite 36-14 has sufficient U concentrations to obtain geologically useful U-Pb dates (>0.5 ppm U). Apatite in felsic garnet granulite 36-14 yields U-Pb dates that scatter between 1.6 Ga and 600 Ma (all assuming a Stacey and Kramers common-Pb composition; Figures 3c and 3d). Most of the apatite in mafic garnet granulite 01-95 has relatively low U (<2 ppm U) and does not produce useful U-Pb dates, but 13 spots with >2 ppm U yield common-Pb corrected dates between 700 Ma and 300 Ma (Figures 3c and 3d). Mafic garnet granulite 79-14 contains apatite with common-Pb corrected U-Pb dates that range from 2.0 Ga and 400 Ma (Figures 3c and 3d). Many apatite grains from xenolith 01-95 contain monazite exsolution lamellae (confirmed by EDS and BSE images; see Figure 3c), and mixing between apatite and monazite is apparent in trace element versus U-Pb date patterns. Spot analyses older than 1.1 Ga define a linear array, with the 2.0 Ga endmember of this array characterized by greater $(Gd/Yb)_N$ ratios and higher Th/U ratios (Figures 3c and 3d).

15252027, 2022, 10, Downloaded from https://agupubs.onlinelibrary.wiley.com/doi/10.1029/2022GC010497 by Cochrane France, Wiley Online Library on [21/10/2022]. See the Terms and Conditions (https://onlinelibrary.wiley.com/terms-and-conditions) on Wiley Online Library for rules of use; OA articles are governed by the applicable Creative Commons License

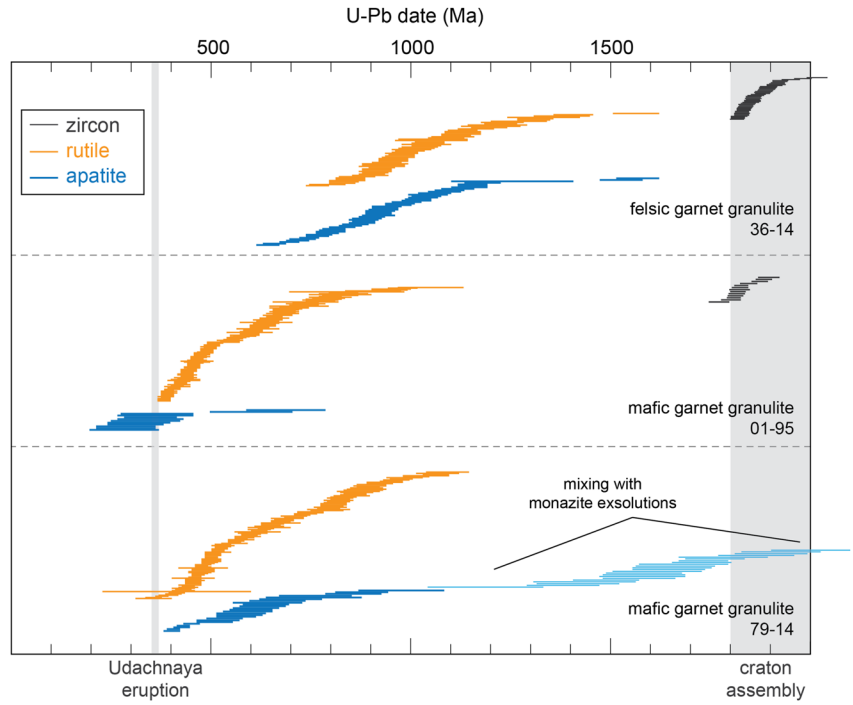


Figure 4. Comparison of zircon, rutile, and apatite U-Pb dates for garnet granulite xenoliths 36-14, 0195, and 79-14. The width of each bar is the 2σ uncertainty of each datum. In the case of mafic garnet granulite 79-14, the mixed apatite-monazite analyses are depicted as lighter blue bars. Note the general overlap between rutile and apatite U-Pb dates. The vertical gray bars represent timing of Paleoproterozoic craton assembly and Late Devonian Udachnaya kimberlite eruption.

Rutile from the garnet granulite xenoliths shows significant age variability. In felsic granulite 36-14 rutile the oldest common-Pb corrected U-Pb date is ca. 1.6 Ga and the youngest date is ca. 760 Ma. Within each grain Zr-in-rutile temperatures are internally coherent, but temperatures vary among different grains (740°C–810°C, assuming a pressure of 1.3 GPa; Figure 3e). Mafic granulites 01-95 and 79-14 both have common-Pb corrected U-Pb dates that range from ca. 1.1 Ga to 360 Ma. Like the felsic garnet granulite, Zr-in-rutile temperatures in both samples are internally consistent but differ between grains (700°C–940°C at 1.2 GPa for sample 01-95 and 820°C–840°C at 0.8 GPa for sample 79-14). Rutile in mafic garnet granulite 01-34 has low U (<0.5 ppm) and produces common-Pb corrected dates with large uncertainties between 500 and 1,600 Ma (Figure 3e). Zr-in-rutile temperatures for this sample are fairly uniform at 875°C–890°C (assuming a pressure of 1.5 GPa). Where present, coexisting apatite usually displays a similar range of U-Pb dates as observed in rutile (Figure 4).

Of the analyzed samples, granulites 36-14 and 01-95 contain rutile with enough U (<1 ppm) to produce robust U-Pb age depth profiles. In mafic garnet granulite 01-95, common-Pb corrected U-Pb date and Pb* concentration profiles increase linearly from 360 Ma at the rim to 1.2 Ga–600 Ma dates at the bottom of the pit (though two profiles are wholly 360 Ma throughout the profile; Figure 6). The outermost 1–2 μm portions of some rutile grains in mafic garnet granulite 01-95 show greater concentrations of U, Pb_c, Zr, and Hf than in the interiors. Beyond the discrete rims, U, Al, and Zr gradually increase toward the grains' interior over a distance of 5–8 μm whereas all other elements show no significant variations with depth (Figure 6). Rutile depth profiles for felsic garnet granulite 36-14 have common-Pb corrected U-Pb dates and Pb* concentrations that gradually increase from the rim toward the grain interior over a distance of 4–6 μm (Figure 6); U-Pb dates at the outermost rim approach the 360 Ma eruption age. In felsic garnet granulite 36-14, rutile depth profiles show that Al concentrations also gradually increase toward the grain interior over 2–8 μm depths (Figure 6). Silicon and Fe also vary, showing relatively higher concentrations on the rims that decrease toward the core (Figure 6). All other trace-elements are largely invariant with depth.

15252027, 2022, 10, Downloaded from https://agupubs.onlinelibrary.wiley.com/doi/10.1029/2022GC010497 by Cochrane France, Wiley Online Library on [21/10/2022]. See the Terms and Conditions (https://onlinelibrary.wiley.com/terms-and-conditions) on Wiley Online Library for rules of use; OA articles are governed by the applicable Creative Commons License

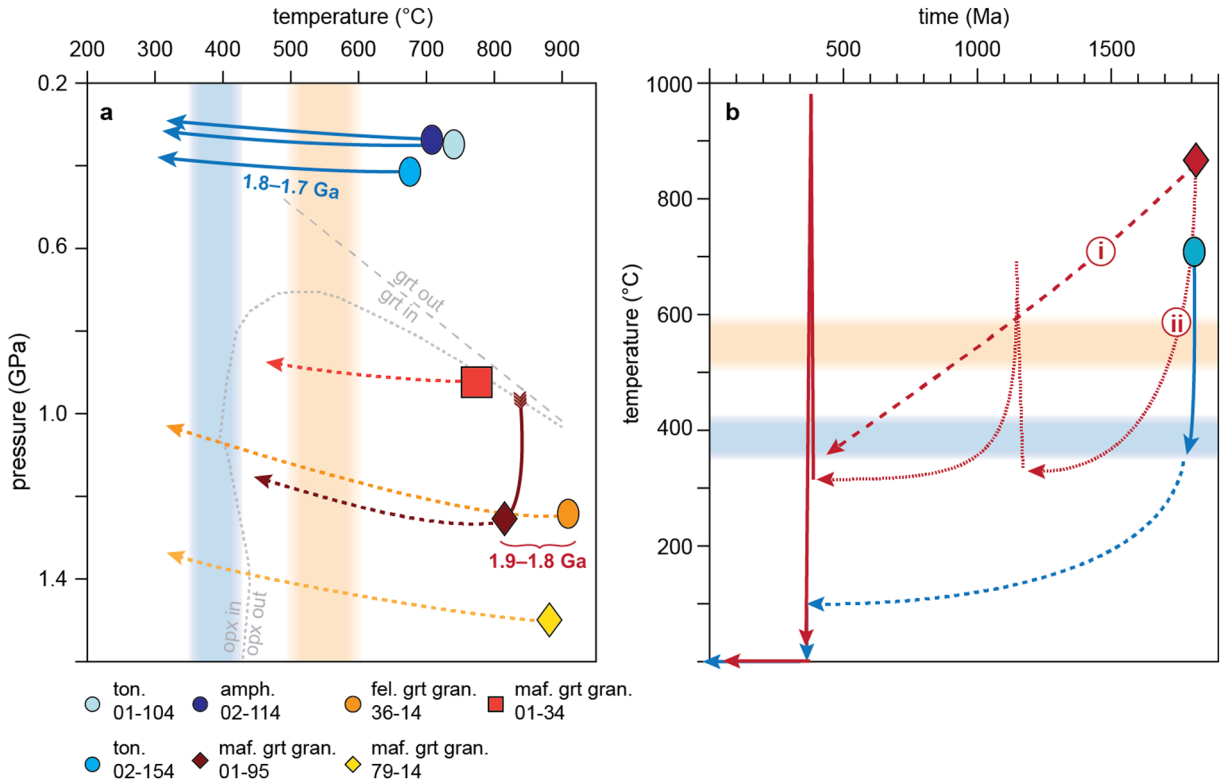


Figure 5. Summary of possible *P-T-t* paths. (a) Schematic *P-T* evolution of the xenoliths. Polygons represent the peak *P-T* conditions determined by the intersections of endmember phase equilibria. Garnet and orthopyroxene stability fields for mafic rocks shown in back. Vertical blue and orange bars represent nominal Pb closure temperatures for apatite and rutile, respectively. In all of the xenoliths, the preservation of apatites older than the 360 Ma eruption age of the Udachnaya kimberlite pipe requires that the rocks cooled below ~400°C at some point in their history. Light gray boundaries denote stability fields of garnet and orthopyroxene determined by Perple_X. (b) Endmember T-t paths (upper crust in blue and lower crust in red). The upper crust cools below apatite Pb closure shortly after 1.8–1.9 Ga craton amalgamation and remains unperturbed ever since. The lower crust could have undergone slow cooling from 1.9 to 1.8 Ga until entrainment (path i) or may have experienced punctuated heating throughout its history (path ii). These endmember scenarios are tested with rutile depth profiling.

6. Discussion

6.1. Metamorphic Histories

In order to link the thermal histories of the xenoliths to heat fluxes in the lithosphere, it is necessary to evaluate what portions of the xenoliths' *P-T* history correspond to thermal conditions shortly prior to eruption (ca. 360 Ma) versus older episodes of metamorphism (e.g., during Proterozoic craton amalgamation). The tonalite and amphibolite xenoliths contain zircon with concordant Archean U-Pb dates and apatite with solely Paleoproterozoic U-Pb dates (Figure 3). The data suggest that these rocks formed in the Archean and were later heated to temperatures high enough to fully reset the apatite (e.g., >700°C for >1 Myr) or recrystallized apatite during ca. 1.8 Ga amalgamation of the Siberian craton (Moyen et al., 2017; Paquette et al., 2017; Rosen et al., 2006). Of prime relevance, the presence of 1.8–1.7 Ga apatite in these rocks implies rapid cooling from 700°C to 750°C to below 400°C–450°C (nominal Pb closure temperature assuming 50–200 μm diameter grains and relevant cooling rates of 1°C–10°C/Myr) at 0.4–0.5 GPa, or 15–20 km depth. These rocks remained below 400°C–450°C and did not experience significant re-heating since 1.8–1.7 Ga (Figure 5b).

Establishing *P-T* paths for high-pressure granulites like those investigated in this study is difficult given the propensity of cation-exchange thermometers to be more affected by retrogression than net-transfer reactions (e.g., Frost & Chacko, 1989; Pattison & Bégin, 1994). The 0.8–1.5 GPa equilibration pressures (or 30–60 km depth) determined from pseudosection modeling and GADS/GAHS thermobarometry likely reflect (near) peak metamorphic conditions at 1.9–1.8 Ga—as evidenced by HREE depletions in zircon (high $(Gd/Yb)_N$) that indicate garnet crystallization at this time (Figure 3a; see also M. Y. Koreshkova et al., 2011)—and need not correspond to their position in the deep crust at 360 Ma (Figure 5a). The cooler 700°C–750°C temperatures recorded by

15252027, 2022, 10, Downloaded from https://agupubs.onlinelibrary.wiley.com/doi/10.1029/2022GC010497 by Cochrane France, Wiley Online Library on [21/10/2022]. See the Terms and Conditions (https://onlinelibrary.wiley.com/terms-and-conditions) on Wiley Online Library for rules of use; OA articles are governed by the applicable Creative Commons License

10.1029/2022GC010497

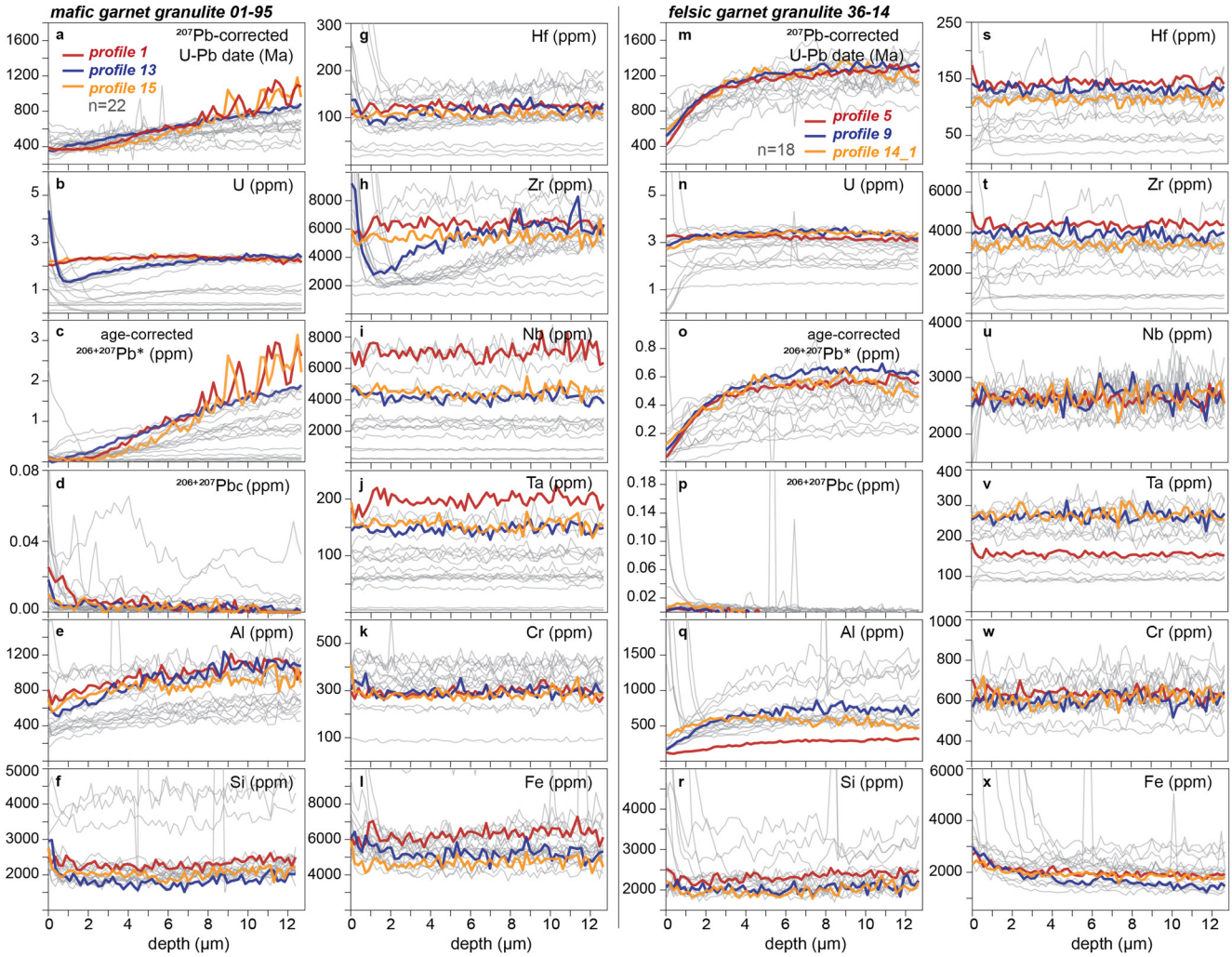


Figure 6. Rutile laser ablation split stream depth profiles. For each sample, three representative profiles are colored (red, blue, and yellow). The other profiles are shown in gray. (a–l) Depth profiles in mafic garnet granulite 01-95 reveal rims enriched in U, Si, Hf, and Zr; elements like U, Pb*, Al, Hf, and Zr show increase gradually toward the interior, whereas other elemental profiles remain flat. (m–x) In felsic garnet granulite 36-14, Pb*, Al, and Fe increase gradually with depth whereas all other elements are invariable with depth.

Fe-Mg exchange thermometry in garnet and pyroxene rims indicate cooling that may correspond to some amount of decompression/exhumation. The cooler rim temperatures, however, are also unlikely to represent ambient temperatures at 360 Ma, but instead reflect closure of diffusional Fe-Mg exchange between garnet and pyroxene (Harley, 1989). In this regard, the U-Pb system in rutile and apatite, which undergo diffusional closure at significantly cooler temperature (Smye et al., 2018), provide further insights into the thermal evolution of the Udachnaya lower crust.

In garnet granulite xenoliths, rutile and apatite record dates that are significantly younger than the well-documented 2.0–1.8 Ga period of craton amalgamation recorded in zircon (Figure 4). In particular, the oldest U-Pb rutile dates from garnet granulite xenoliths 79-14, 01-95, and 36-14 are 1.6–1.1 Ga (Figure 4). These dates could be interpreted as the time when the rocks cooled below rutile Pb closure following slow cooling from 1.8 Ga or a discrete re-heating event at 1.6–1.1 Ga. If the rocks underwent slow cooling through the Pb closure temperature of rutile and apatite since 1.8 Ga, one would predict that apatite dates would be as young or younger than rutile dates (calculated Pb closure temperatures for rutile are 500°C–600°C and for apatite are 350°C–450°C using relevant 50–500-μm-radius grains and cooling rates of 0.01°C–0.1°C/Myr). In mafic garnet granulite 01-95, apatite U-Pb dates are consistently younger than the oldest rutile dates, and in felsic garnet granulite 36-14, the oldest apatite U-Pb dates are within uncertainty of the oldest 1.6 Ga rutile date (Figure 4). The exception is mafic garnet

15252027, 2022, 10, Downloaded from https://agupubs.onlinelibrary.wiley.com/doi/10.1029/2022GC010497 by Cochrane France, Wiley Online Library on [21/10/2022]. See the Terms and Conditions (https://onlinelibrary.wiley.com/terms-and-conditions) on Wiley Online Library for rules of use; OA articles are governed by the applicable Creative Commons License

15252027, 2022, 10, Downloaded from https://agupubs.onlinelibrary.wiley.com/doi/10.1029/2022GC010497 by Cochrane France, Wiley Online Library on [21/10/2022]. See the Terms and Conditions (https://onlinelibrary.wiley.com/terms-and-conditions) on Wiley Online Library for rules of use; OA articles are governed by the applicable Creative Commons License

granulite 79-14, where about half of the apatite dates are significantly older than rutile dates (up to 2.0–1.8 Ga; Figure 4). The presence of monazite exsolution lamellae in apatite from this sample complicates comparisons between apatite and rutile U-Pb dates; because Pb diffusion in monazite occurs at significantly higher temperatures than apatite (Cherniak et al., 2004), any spot analyses incorporating monazite will produce a spread of U-Pb dates unrelated to thermally mediated volume diffusion. Based on trends in U-Pb date versus Gd/Yb and Th/U ratios, we conclude that ca. 2.0 Ga U-Pb dates represent the timing of monazite exsolution formation; apatite spot dates >1.1 Ga are due to mixed monazite/apatite analyses and are therefore not geologically meaningful. Accounting for this, the oldest apatite U-Pb date in mafic garnet granulite 79-14 is younger than the oldest rutile U-Pb date.

Based on apatite and rutile U-Pb dates, we suggest that the ca. 1.6–1.1 Ga upper age intercepts represent Mesoproterozoic re-heating of the lower crust by a discrete thermal event, and are not due to slow monotonic cooling through rutile/apatite Pb closure since 1.8 Ga. In support of this interpretation, we note that the oldest apatite and rutile U-Pb dates in felsic garnet granulite 36-14 are both 1.6 Ga, requiring rapid cooling through the nominal Pb closure temperatures of both phases (Figure 5b). No 1.6–1.1 Ga crystallization dates have been documented previously in outcrops or in xenoliths from the central Siberian craton (M. Koreshkova et al., 2009; Paquette et al., 2017; Priyatkina et al., 2016), with the exception of rift-related dike swarms in the Anabar shield and Olenek uplift that record similar ages (see Cherepanova et al., 2013; Gladkochub et al., 2012; and references therein). We speculate that a similar dike emplacement event occurred around Udachnaya at 1.6–1.1 Ga, creating a thermal pulse that heated the lower crust above the Pb closure temperatures of rutile and apatite (akin to resetting of rutile in Slave craton xenoliths by dike swarm intrusion; Davis, 1997). The spread of rutile U-Pb dates down to 360 Ma provides further insight into the thermal evolution of the deep crust following the Mesoproterozoic.

6.2. Re-Heating the Lower Crust?

The objective of multi-element depth profiling is to ascertain whether age and geochemical gradients within minerals are a result of thermally mediated volume diffusion or re-/neo-crystallization. If Pb was diffusing out of rutile during slow cooling in the lower crust over billion year timescales, this would imply residence at 500°C–600°C (temperatures of partial Pb retention in rutile) prior to eruption (path I in Figure 5b) (e.g., Schmitz & Bowring, 2003; T. Blackburn et al., 2011). On the other hand, Pb-loss could have been induced by a thermal event associated with kimberlite magmatism, which would imply long-term ambient lower crustal temperatures cooler than the nominal Pb closure temperature of rutile (path ii in Figure 5b). A third alternative is that gradients reflect re-/neo-crystallization in the deep crust during or shortly before kimberlite magmatism.

In order to evaluate the different scenarios discussed above, we calculated the inverse error functions of the normalized Pb and trace elements gradients in the 22 rutile depth profiles in mafic garnet granulite 01-95 and 18 rutile depth profiles in felsic garnet granulite 36-14. Gradients produced by thermally mediated volume diffusion are expected to conform to an error function—reflected in the linearity of the inverse error function—and the slopes of the gradients are predicted to scale by $\frac{1}{\sqrt{4\times D(T)\times t}}$ (Crank, 1979; see also Section 4.4). Figure 7 illustrates representative depth profiles of rutile in mafic garnet granulite 01-95 (profile 13) and felsic garnet granulite 36-14 (profile 9). In profile 13 of mafic garnet granulite 01-95, a 1-µm-thick rim is followed by monotonous increases in Pb*, Al, and Zr toward the grain interior (Figure 7a); the latter portion of the profiles conform to an error function, but the corresponding slopes yield values that all overlap within uncertainty (Figure 7b). Similarly, rutile depth profile 9 from felsic garnet granulite 36-14 shows Pb* and Al gradients that also follow an error function with indistinguishable slopes (Figure 7d). The available experimentally determined diffusivities for Al, Pb, and Zr predict decoupling of these elements across relevant crustal temperatures ($D_{Al} \approx 1E{-}9{*}D_{Pb*}$ and $D_{Al} \approx 1E{-}9{*}D_{Zr}$ at 600°C, e.g., Cherniak and Watson (2019) and references therein). Therefore, if the gradients captured in the rutile interiors all formed by the same process, they cannot be explained by diffusion over billions of years as this would produce systematic variability in the slopes in Figures 7b and 7d. While it is possible that the Al profiles developed during an earlier episode of intense heating and the Pb* profile during later slow cooling, coincidentally producing gradients show nearly identical inverse error functions, we argue that the depth profiles capture rutile crystallization and/or shorter-term heating near the time of entrainment in the kimberlite.

We propose that partial U-Pb resetting of rutile from the Udachnaya lower crustal xenolith suite reflects transient heat advection from and interactions with melts/fluids prior to kimberlite eruption. The observation that different rutile depth profiles exhibit different U-Pb dates and elemental concentrations at the rim suggests flux-limited

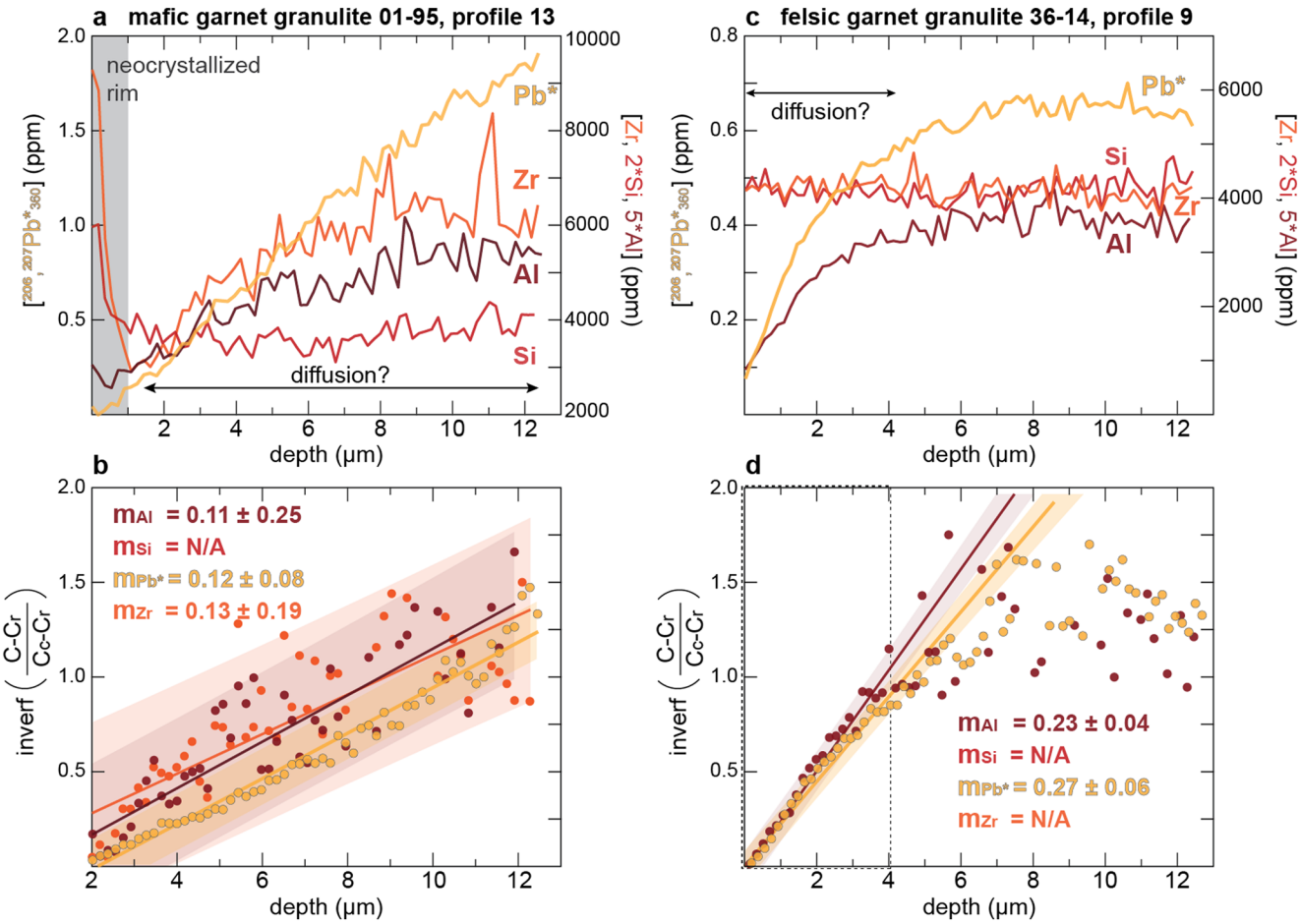


Figure 7. Representative profiles in mafic garnet granulite 01-95 and felsic garnet granulite 36-14. (a and b) In profile 13 of mafic garnet granulite 01-95, a 1-μm-thick rim is distinguished by elevated Zr (see also Figure 6). Beyond this rim, there is monotonous increases in Al, Zr, and Pb* toward the grain interior that could be related to thermally mediated volume diffusion. This latter portion of the profiles conform to an error function, but the corresponding slopes yield values that all overlap within uncertainty (panel b). (c and d) Similarly, rutile depth profile 9 from felsic garnet granulite 36-14 (panels (c and d)) shows Pb* and Al gradients also follow an error function form and produce indistinguishable slope values. Data included in the dashed area were used to calculate slopes. Thermally mediated volume diffusion over billions of years would be expected to produce differences in the slopes of the inverse error functions that vary by $\frac{1}{\sqrt{4 \times D(T) \times t}}$. The profiles therefore correspond to transient heating or (re)crystallization immediately prior to eruption.

element transport at the grain boundary (Kohn et al., 2016; Smye et al., 2018). The development of elemental gradients could have been controlled by adjacent phases (garnet, pyroxene, feldspar) or a fluid phase that imposed different boundary conditions across at the grain edge. The involvement of fluids is supported texturally by the presence of pockets of fine-grained material and secondary biotite in the xenoliths, which may be remnants of a melt/fluid (Figure 2). There is also ample evidence for metasomatism in the Udachnaya peridotite xenolith suite (Agashev et al., 2013; Boyd et al., 1997; Golovin et al., 2018; Ionov et al., 2010; M. Y. Koreshkova et al., 2011; V. Shatsky et al., 2008). Agashev et al. (2013) identified multiple episodes of metasomatism in the peridotite xenoliths: carbonatite metasomatism (addition of Ca, Al, and LREE); silicate melt metasomatism (enrichment of REE, Y, and Zr resulting in formation of garnet and clinopyroxene in otherwise highly depleted peridotites; see also Boyd et al. (1997)), including enriched-basaltic melt metasomatism (local enrichment of Fe and Ti). In addition, Golovin et al. (2018) described Na-K-Ca-rich melt inclusions in olivine from sheared peridotite xenoliths that resulted from interactions with primitive kimberlite magmas in the mantle prior to eruption. Regarding Udachnaya granulite xenoliths, Koreshkova et al. (2011) noted that kimberlite melt interactions are required to account for bulk enrichments of LREE, Th, and U (with contributions from kimberlite-related fluids; Kamenetsky et al., 2007).

15252027, 2022, 10, Downloaded from https://agupubs.onlinelibrary.wiley.com/doi/10.1029/2022GC010497 by Cochrane France, Wiley Online Library on [21/10/2022]. See the Terms and Conditions (https://onlinelibrary.wiley.com/terms-and-conditions) on Wiley Online Library for rules of use; OA articles are governed by the applicable Creative Commons License

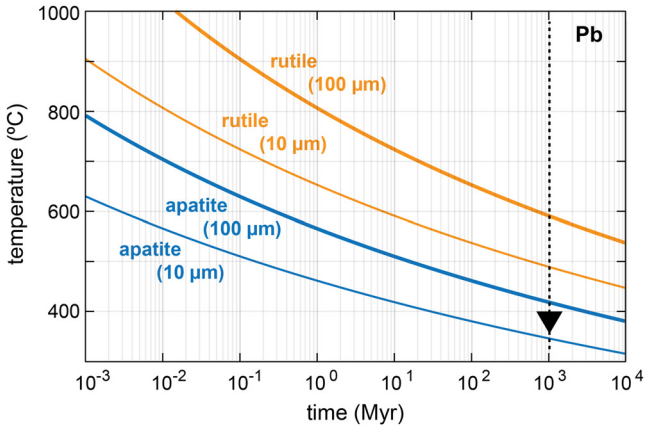


Figure 8. Characteristic length scales (10 and 100 μm contours) of diffusion of Pb for apatite (blue) and rutile (orange). Rutile and apatite are expected to experience different degrees of Pb diffusion across all relevant temperatures and durations of heating. In order to preserve 1.1 Ga rutile and apatite dates, lower-crustal temperatures were below 400°C (down arrow at 10^3 Myr). Rutile Pb diffusivity data from Cherniak (2000) and apatite Pb diffusivity data from Cherniak et al. (1991).

The involvement of one or more of the putative metasomatic media discussed above could be responsible for the development of the complex age and elemental patterns observed in the rutile depth profiles. Trace-element rutile-melt partition coefficients—especially the high field strength elements like Zr, Hf, Nb, Ta—depend greatly on melt composition (Foley et al., 2000; Klemme et al., 2005; and references therein). For example, Klemme et al. (2005) note the compatibility of high field strength elements in rutile over silicate melt with an andesitic or rhyolitic composition. Neither of these melt compositions would be wholly relevant to the Udachnaya xenoliths as they are too silicic and viscous, but we speculate that the enriched U, Hf, and Zr at the rims relative to the rutile interior could have resulted from a combination of the melt compositions documented in other Udachnaya xenoliths. An additional consideration is that portions of the rutile depth profiles record diffusion (see Figures 7a and 7c) in response to heating at relatively high temperatures and over short time scales.

Thin rims (1–2 μm) observed on rutile in mafic garnet granulite 01-95 are enriched in U, Pb_c, Hf, and Zr. We interpret this feature as reflecting neo- or re-crystallization of rutile associated with precursory kimberlitic magmatism. This process is distinct from the eruption process itself because: (a) timescales of transport to the surface are too short to cause significant Pb diffusion (Doucet et al., 2014; Schmitz & Bowring, 2003; Spera, 1984); and (b) shallower tonalite and amphibolite xenoliths from the same kimberlite pipe have apatite with undisturbed Paleoproterozoic U-Pb isochrons (Figures 3c and 3d). The elevated Zr concentrations in the 01-95 rutile rims indicate heating to high temperatures prior to eruption (e.g., 9,000 ppm Zr in profile 13 equates to >1000°C, and higher still in other profiles; Figure 6). Thus, in addition to metasomatism, it is probable that such extreme temperatures prior to eruption induced Pb loss. Assuming that a portion of the rutile Pb profiles does reflect thermally mediated volume diffusion (Figure 7), bounds can be placed on the duration of heating. The observed Pb* gradients in rutile from mafic garnet granulite 01-95 are consistent with average heating time-scales of <18, <3, and <0.6 Myr at 900°C, 1000°C, and 1100°C, respectively; time-scales of heating based on Pb* profiles in rutile from felsic garnet granulite 36-14 are <4, <0.6, and <0.1 Myr at 900°C, 1000°C, and 1100°C, respectively. Because slower-diffusing Al shows similar gradients to Pb* in the rutile profiles (Figure 6), the time-scales of heating calculated from Pb gradients are maxima. Nonetheless, the transient nature of this event is consistent with timescales of advective heating prior to eruption proposed for other xenolith suites, such as those from the North Atlantic craton (Smit et al., 2016), Kaapvaal craton (Jollands et al., 2018) and Tibetan Plateau (Hacker et al., 2000).

If deep crustal heating was depth-dependent, then samples with greater U-Pb resetting resided at greater depths relative to those with minimal overprinting (e.g., the mafic granulites were deeper than the felsic granulites; Figure 4). However, there is no correlation between the extent of rutile U-Pb resetting and peak pressure, and advective heating may have been heterogeneous. This inference is supported by data on Udachnaya mantle xenoliths that suggest similar heterogeneous heating in the mantle lithosphere (e.g., Liu et al., 2022).

Finally, if the U-Pb heterogeneity was caused by processes that operated immediately preceding kimberlite eruption, the preservation of Proterozoic rutile and apatite dates indicates that the deep crust of the Siberian craton generally resided at temperatures cool enough that Pb was not actively diffusing out of the rutile and apatite crystal lattice prior to this late-stage heating. For the typical 50–200 μm-wide apatite grains this translates to temperatures below 400°C for ~1 Gyr (Figure 8).

6.3. Crustal Heat Production Models for the Siberian Craton

The data discussed above provide new temperature constraints that can be used to calculate crustal heat production. Previous approaches to determining crustal heat production include using measured abundances of U, Th, and K in lower-crustal granulite terranes exposed at the surface or reconstructed from xenoliths (e.g., Gruber et al., 2021; Nicolaysen et al., 1981; Sandiford et al., 2002). Each of these approaches has advantages and disadvantages. The former is accessible and enables extensive sampling, but granulites terranes may have only resided

15252027, 2022, 10, Downloaded from https://agupubs.onlinelibrary.wiley.com/doi/10.1029/2022GC010497 by Cochrane France, Wiley Online Library on [21/10/2022]. See the Terms and Conditions (https://onlinelibrary.wiley.com/terms-and-conditions) on Wiley Online Library for rules of use; OA articles are governed by the applicable Creative Commons License

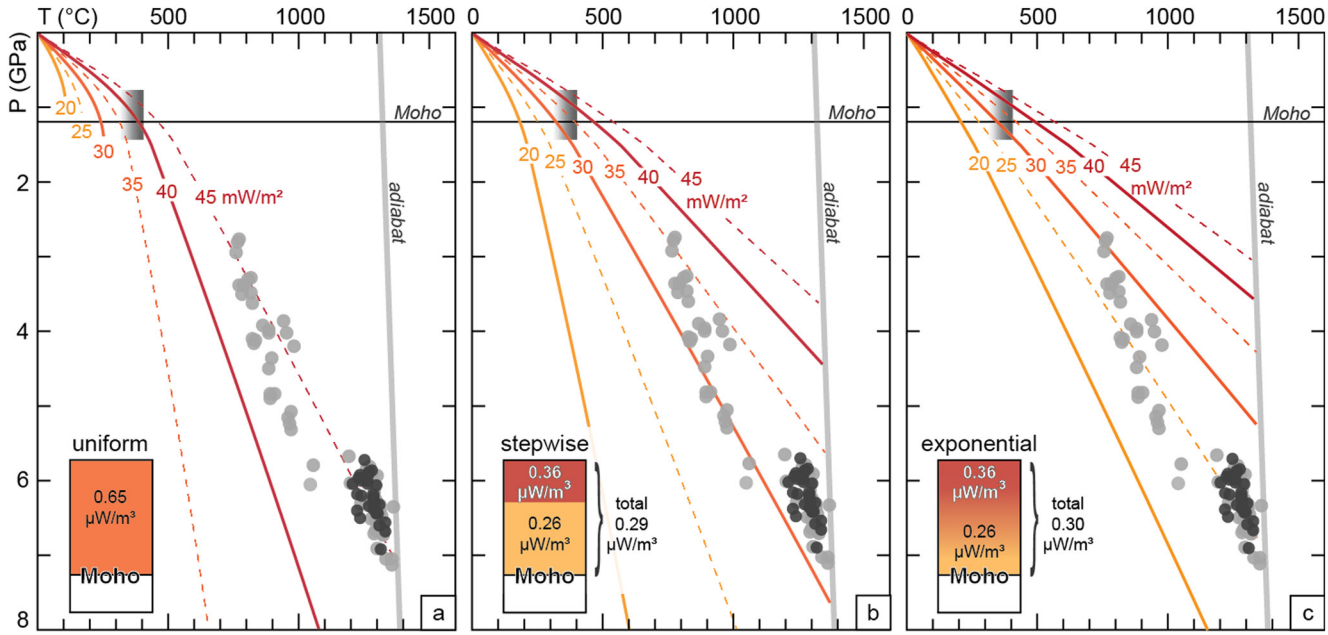


Figure 9. Conductive geotherm models. Model A assumes uniform crustal heat production (average Archean heat production value of Jaupart and Mareschal (2014)). Model B assumes a stepwise change in heat production at 15 km. Model C assumes an exponential decrease in crustal heat production. All models employ heat production value of 0.006 µW/m^3 for the mantle lithosphere (after McIntyre et al., 2021). Moho is at 45 km (after Cherepanova et al., 2013). Garnet peridotite *P-T* data are shown in gray, with darker gray spots representing sheared peridotites (data from Liu et al. (2022)). In models (B and C), the surface heat flow values of 20–35 mW/m^2 are consistent with preservation of Proterozoic apatite and rutile U-Pb dates (<400°C, represented by the gray bar at 0.8–1.4 GPa) and the peridotite *P-T* data. These surface heat flow values are generally higher than the average surface heat flow measurements around Udachnaya (19 ± 3 mW/m^2).

transiently in the mid–deep crust and may not be representative of the lower crust (e.g., Bohlen & Mezger, 1989). The latter provides in situ samples of deep crust, but suffers from unquantifiable uncertainties because it is unknown how representative a xenolith suite is of a crustal column in general (i.e., whether the whole column was sampled and if it was sampled in direct proportion that it exists within the crust). The approach we take exploits the temperature bounds imposed by U-Pb thermochronology to constrain heat fluxes near the Moho. That is, our data require long-term Moho temperatures below 400°C (temperatures cool enough to preserve Mesoproterozoic rutile and apatite U-Pb dates).

As a secondary check, we compare permissible geothermal gradients to *P-T* data from garnet peridotite xenoliths also entrained by the Udachnaya kimberlite(e.g., Liu et al., 2022; R. L. Rudnick et al., 1998). If the garnet peridotite xenoliths were in equilibrium at ambient mantle lithosphere conditions, any geotherm encompassing the mantle xenolith data would also yield Moho temperatures cooler than ~400°C (i.e., temperatures for the lower crust and Moho should be consistent with closed-system behavior of Pb in rutile and apatite).

We assess different heat production models for the lithospheric column at Udachnaya using steady-state one-dimensional conductive geotherms (following Hasterok and Chapman (2011) and Furlong and Chapman (2013)). Our goal is not to determine the exact crustal heat production value for Udachnaya, but rather to evaluate general trends in geotherms that match the available xenolith data. We evaluate three different distribution models of heat production within the crust: (a) uniform crustal heat production; (b) stepwise decrease in crustal heat production with depth; and (c) exponential decrease in heat production with depth (Figure 9).

In model A, we chose a uniform average Archean crustal heat production of 0.65 µW/m^3 (Jaupart & Mareschal, 2014). In model B, we calculate heat production values based on whole-rock measurements of U, Th, and K in crustal xenoliths (Moyen et al., 2017) and adopt a stepwise change in heat production assuming two layers: an upper crust (0–15 km) consisting of tonalite only and lower crust (15–45 km). The average upper crustal tonalite heat-production is 0.36 µW/m^3, whereas the lower crustal average heat production of mafic granulites is 0.26 µW/m^3 for a total crustal heat production of 0.29 µW/m^3. These heat production values are based on bulk whole-rock measurements, which we note are likely biased toward higher values given the likelihood of contamination of the whole rocks by kimberlite magma or related fluids (Golovin et al., 2018, 2020; Kamenetsky

15252027, 2022, 10, Downloaded from https://agupubs.onlinelibrary.wiley.com/doi/10.1029/2022GC010497 by Cochrane France, Wiley Online Library on [21/10/2022]. See the Terms and Conditions (https://onlinelibrary.wiley.com/terms-and-conditions) on Wiley Online Library for rules of use; OA articles are governed by the applicable Creative Commons License

15252027, 2022, 10, Downloaded from https://agupubs.onlinelibrary.wiley.com/doi/10.1029/2022GC010497 by Cochrane France, Wiley Online Library on [21/10/2022]. See the Terms and Conditions (https://onlinelibrary.wiley.com/terms-and-conditions) on Wiley Online Library for rules of use; OA articles are governed by the applicable Creative Commons License

et al., 2007; M. Koreshkova et al., 2009). Model C assumes an exponential decrease in heat production, starting with the average tonalite heat-production at the surface and grading to an average mafic granulite value at 45 km depth for an integrated crustal heat production of 0.30 $\mu W/m^3$. All of the models utilize a mantle lithosphere heat production value of 0.006 $\mu W/m^3$ (after McIntyre et al., 2021), a Moho depth of ~45 km (Cherepanova et al., 2013), and are calculated with fixed surface heat flow values between 20 and 50 mW/m^2 (encompassing the range observed in cratons globally; Jaupart & Mareschal, 2014).

Some interesting observations derive from these modeled geotherms. First, the geotherms encapsulating the peridotite *P-T* data suggest Moho temperatures that are cooler than the temperature bounds suggested by apatite and rutile U-Pb dates (<400°C; Figure 8). Notably, the cool geotherms are consistent with relatively deep Curie depth estimates for the Siberian craton (>35 km; Gard & Hasterok, 2021), highlighting potential magnetization below the Moho (Ferré et al., 2013). Second, in all three models the Udachnaya peridotite *P-T* data require geotherms that are uniformly higher than the measured surface heat flow value of 19 ± 3 mW/m^2 (represented approximately by the 20 mW/m^2 geotherms in Figure 9). The peridotite xenolith *P-T* data do indeed reflect some lithospheric heating prior to eruption (see Liu et al., 2022), such that the ambient geotherm at 360 Ma should lie closer to the cooler geotherms (Figure 9). Even so, reconciling the Udachnaya peridotite *P-T* data with the observed low surface heat flow around Udachnaya would require substantial cooling of the lower crust since kimberlite emplacement 360 Ma; the secular decay of radioactive elements alone could not account for this (~100°C/Gyr; Jaupart et al., 2016). The Siberian xenolith data are, however, consistent with the global average surface heat flow range of 20–50 mW/m^2 for cratons (Jaupart et al., 2016). Given these considerations, we assert that surface heat flow measurements made in the central Siberian craton are inaccurate, having been potentially compromised by the thick and permeable sedimentary and volcanic cover (Cherepanova et al., 2013), largely infiltrated by brines (Alexeev et al., 2007, 2022; Kitayama et al., 2021), or the chilling effect of Pleistocene glaciations (Birch, 1948).

Of the three crustal models, the constraints from both lower crustal temperatures and mantle xenolith *P-T* arrays are best matched by models B and C (Figure 9), which have extremely low total crustal heat production in the Siberian craton, on the order of ~0.3 $\mu W/m^3$. This could reflect a bulk mafic crust composition (e.g., R. L. Rudnick & Gao, 2014) or extensive depletion of heat-producing elements during high-temperature metamorphism and melt extraction associated with cratonization (e.g., Carlson et al., 2005). The presence of lower-crustal felsic granulites at Udachnaya and nearby sites require some amount of silicic material at depth (e.g., Moyen et al., 2017; M. Y. Koreshkova et al., 2011; Shatsky et al., 2019). Previous studies have shown that accessory phases in high-grade felsic rocks retain Th even after undergoing extensive melt depletion (e.g., Alessio et al., 2018; Bea, 1996; R. L. Rudnick & Fountain, 1995), such that high heat-producing felsic lithologies may be subordinate to mafic lithologies in the deep crust of the Siberian craton.

7. Conclusions

New laser ablation split-stream U-Pb and trace-element data from accessory phases in xenoliths from the ca. 360 Ma Udachnaya kimberlite, Siberian craton, show that the U-Pb system is sensitive to transient heating of the lower crust and not just slow cooling. Length-scales of U-Pb and trace element gradients revealed by depth profiling of rutile suggest that depth-dependent heating of the deep crust occurred for <1 Myr before eruption. Preserved Mesoproterozoic dates in both apatite and rutile long-term lower-crustal temperatures were cool enough that Pb was not actively diffusing out of the both phases (<400°C). The lower-crustal temperature bounds imparted by these data are consistent with *P-T* arrays of Udachnaya peridotite xenoliths that suggest relatively cool geothermal gradients, signifying that the mantle xenoliths accurately capture the thermal state of the lithosphere prior to eruption. Combined, the xenolith data imply low crustal heat production for the Siberian craton (~0.3 $\mu W/m^3$). Although exceedingly low, such values still produce surface heat flow values higher than those measured around Udachnaya (average 19 mW/m^2), suggesting that the surface heat flow measurements are too low (possible compromised by thick sedimentary cover and deep regional aquifers). Collectively, the xenolith data support low crustal heat production in the Siberian craton, implying a relatively mafic bulk crust composition or a HPE-depleted felsic bulk crust.

Data Availability Statement

The data are archived in the DRYAD data repository and the DOI will be made publicly accessible upon publication of this manuscript (https://doi.org/10.25349/D94K79).

Acknowledgments
The authors dedicate this work to the memory of Nikolay V. Sobolev, a pioneer in xenolith studies of the Siberian craton. He generously provided some of the new xenoliths described here (79-XX samples). The authors thank Gareth Seward and Andrew Kylander-Clark for assistance with SEM/electron probe micro analyzer and LASS analyses, respectively. Thanks also go to Bradley Hacker, Joshua Garber, Matthew Rioux, and Zachary Eilon for productive discussions throughout the course of the study; and editor Peter van der Beek and reviewers Andrew Smye, Terrence Blackburn, and David Chew for constructive comments that improved the manuscript. Funded by the University of California, Santa Barbara, NSF-EAR-1650260 to Rudnick and Cottle, an NSF graduate research fellowship to Apen, and an INSU-CNRS grant to Ionov. Golovin acknowledges support from the Russian Federation state assignment project of IGM SB RAS; Korsakov acknowledges Russian Science Foundation Grant 18-17-00186.

References

Agashev, A. M., Ionov, D. A., Pokhilenko, N. P., Golovin, A. V., Cherepanova, Y., & Sharygin, I. S. (2013). Metasomatism in lithospheric mantle roots: Constraints from whole-rock and mineral chemical composition of deformed peridotite xenoliths from kimberlite pipe Udachnaya. *Lithos*, *160–161*(1), 201–215. https://doi.org/10.1016/j.lithos.2012.11.014

Alessio, K. L., Hand, M., Kelsey, D. E., Williams, M. A., Morrissey, L. J., & Barovich, K. (2018). Conservation of deep crustal heat production. *Geology*, *46*(4), 335–338. https://doi.org/10.1130/G39970.1

Alexeev, S. V., Alexeeva, L. P., Borisov, V. N., Shouakar-Stash, O., Frape, S. K., Chabaux, F., & Kononov, A. (2007). Isotopic composition (H, O, Cl, Sr) of ground brines of the Siberian 659 Platform. *Russian Geology and Geophysics*, *48*(3), 225–236. https://doi.org/10.1016/j.rgg.2007.02.007

Alexeev, S. V., Alexeeva, L. P., & Trifonov, N. S. (2022). Equilibrium-non-equilibrium of the brine-kimberlite system in the Udachnaya pipe, Russia, based on physicochemical modeling. *Applied Geochemistry*, *138*(January), 105219. https://doi.org/10.1016/j.apgeochem.2022.105219

Anderson, J. L., & Smith, D. R. (1995). The effects of temperature and f_{O2} on the Al-in-hornblende barometer. *American Mineralogist*, *80*(5–6), 549–559. https://doi.org/10.2138/am-1995-5-614

Apen, F. E., Rudnick, R. L., Cottle, J. M., Kylander-Clark, A. R. C., Blondes, M. S., Piccoli, P. M., & Seward, G. (2020). Four-dimensional thermal evolution of the East African Orogen: Accessory phase petrochronology of crustal profiles through the Tanzanian Craton and Mozambique Belt, northeastern Tanzania. *Contributions to Mineralogy and Petrology*, *175*(11), 97. https://doi.org/10.1007/s00410-020-01737-6

Bea, F. (1996). Residence of REE, Y, Th and U in granites and crustal protoliths; implications for the chemistry of crustal melts. *Journal of Petrology*, *37*(3), 521–552. https://doi.org/10.1093/petrology/37.3.521

Birch, A. F. (1948). The effects of Pleistocene climatic variations upon geothermal gradients. *American Journal of Science*, *246*(12), 729–760. https://doi.org/10.2475/ajs.246.12.729

Blackburn, T. J., Bowring, S. A., Perron, J. T., Mahan, K. H., Dudas, F. O., & Barnhart, K. R. (2012). An exhumation history of Continents over billion-year time scales. *Science*, *335*(6064), 73–76. https://doi.org/10.1126/science.1213496

Blackburn, T., Bowring, S. A., Schoene, B., Mahan, K., & Dudas, F. (2011). U-Pb thermochronology: Creating a temporal record of lithosphere thermal evolution. *Contributions to Mineralogy and Petrology*, *162*(3), 479–500. https://doi.org/10.1007/s00410-011-0607-6

Bohlen, S. R., & Mezger, K. (1989). Origin of granulite terranes and the formation of the lowermost continental crust. *Science*, *244*(4902), 326–329. https://doi.org/10.1126/science.244.4902.326

Boyd, F. R. (1984). Siberian geotherm based on lherzolite xenoliths from the Udachnaya kimberlite, USSR. *Geology*, *12*(9), 528–530. https://doi.org/10.1130/0091-7613(1984)12<528:SGBOIX>2.0.CO;2

Boyd, F. R., Pokhilenko, N. P., Pearson, D. G., Mertzman, S. A., Sobolev, N. V., & Finger, L. W. (1997). Composition of the Siberian cratonic mantle: Evidence from Udachnaya peridotite xenoliths. *Contributions to Mineralogy and Petrology*, *128*(2–3), 228–246. https://doi.org/10.1007/s004100050305

Brey, G. P., & Köhler, T. (1990). Geothermobarometry in four-phase lherzolites II. New thermobarometers, and practical assessment of existing thermobarometers. *Journal of Petrology*, *31*(6), 1353–1378. https://doi.org/10.1093/petrology/31.6.1353

Carlson, R. W., Pearson, D. G., & James, D. E. (2005). Physical, chemical, and chronological characteristics of continental mantle. *Reviews of Geophysics*, *43*(1), 1–24. https://doi.org/10.1029/2004RG000156

Cherepanova, Y., Artemieva, I. M., Thybo, H., & Chemia, Z. (2013). Crustal structure of the Siberian craton and the West Siberian basin: An appraisal of existing seismic data. *Tectonophysics*, *609*, 154–183. https://doi.org/10.1016/j.tecto.2013.05.004

Cherniak, D. J. (2000). Pb diffusion in rutile. *Contributions to Mineralogy and Petrology*, *139*(2), 198–207. https://doi.org/10.1007/PL00007671

Cherniak, D. J. (2010). Diffusion in accessory minerals: Zircon, titanite, apatite, monazite and Xenotime. *Reviews in Mineralogy and Geochemistry*, *72*(1), 827–869. https://doi.org/10.2138/rmg.2010.72.18

Cherniak, D. J., Lanford, W. A., & Ryerson, F. J. (1991). Lead diffusion in apatite and zircon using ion implantation and Rutherford backscattering techniques. *Geochimica et Cosmochimica Acta*, *55*(6), 1663–1673. https://doi.org/10.1016/0016-7037(91)90137-T

Cherniak, D. J., Manchester, J., & Watson, E. B. (2007). Zr and Hf diffusion in rutile. *Earth and Planetary Science Letters*, *261*(1–2), 267–279. https://doi.org/10.1016/j.epsl.2007.06.027

Cherniak, D. J., & Watson, E. B. (2019). Al and Si diffusion in rutile. *American Mineralogist*, *104*(11), 1638–1649. https://doi.org/10.2138/am-2019-7030

Cherniak, D. J., Watson, E. B., Grove, M., & Harrison, T. M. (2004). Pb diffusion in monazite: A combined RBS/SIMS study. *Geochimica et Cosmochimica Acta*, *68*(4), 829–840. https://doi.org/10.1016/j.gca.2003.07.012

Connolly, J. A. D. (2009). The geodynamic equation of state: What and how. *Geochemistry, Geophysics, Geosystems*, *10*(10), Q10014. https://doi.org/10.1029/2009GC002540

Connolly, J. A. D., & Kerrick, D. M. (1987). An algorithm and computer program for calculating composition phase diagrams. *Calphad*, *11*(1), 1–55. https://doi.org/10.1016/0364-5916(87)90018-6

Cottle, J. M., Horstwood, M. S. A., & Parrish, R. R. (2009). A new approach to single shot laser ablation analysis and its application to in situ Pb/U geochronology. *Journal of Analytical Atomic Spectrometry*, *24*(10), 1355. https://doi.org/10.1039/b821899d

Crank, J. (1979). *The mathematics of diffusion*. Oxford University Press.

Davis, W. J. (1997). U-Pb zircon and rutile ages from granulite xenoliths in the Slave province: Evidence for mafic magmatism in the lower crust coincident with Proterozoic dike swarms. *Geology*, *25*(4), 343. https://doi.org/10.1130/0091-7613(1997)025<0343:UPZARA>2.3.CO;2

Davis, W. J., Canil, D., MacKenzie, J. M., & Carbno, G. B. (2003). Petrology and U–Pb geochronology of lower crustal xenoliths and the development of a craton, Slave Province, Canada. *Lithos*, *71*(2–4), 541–573. https://doi.org/10.1016/S0024-4937(03)00130-0

Dodson, M. H. (1973). Closure temperature in cooling geochronological and petrological systems. *Contributions to Mineralogy and Petrology*, *40*(3), 259–274. https://doi.org/10.1007/bf00373790

Doucet, L. S., Ionov, D. A., Golovin, A. V., & Pokhilenko, N. P. (2012). Depth, degrees and tectonic settings of mantle melting during craton formation: Inferences from major and trace element compositions of spinel harzburgite xenoliths from the Udachnaya kimberlite, central Siberia. *Earth and Planetary Science Letters*, *359*(360), 206–218. https://doi.org/10.1016/j.epsl.2012.10.001

15252027, 2022, 10, Downloaded from https://agupubs.onlinelibrary.wiley.com/doi/10.1029/2022GC010497 by Cochrane France, Wiley Online Library on [21/10/2022]. See the Terms and Conditions (https://onlinelibrary.wiley.com/terms-and-conditions) on Wiley Online Library for rules of use; OA articles are governed by the applicable Creative Commons License

Doucet, L. S., Peslier, A. H., Ionov, D. A., Brandon, A. D., Golovin, A. V., Goncharov, A. G., & Ashchepkov, I. V. (2014). High water contents in the Siberian cratonic mantle linked to metasomatism: An FTIR study of Udachnaya peridotite xenoliths. *Geochimica et Cosmochimica Acta*, *137*, 159–187. https://doi.org/10.1016/j.gca.2014.04.011

Edwards, G. H., & Blackburn, T. (2018). Detecting the extent of ca. 1.1 Ga Midcontinent Rift plume heating using U-Pb thermochronology of the lower crust. *Geology*, *46*(10), 911–914. https://doi.org/10.1130/G45150.1

Ferry, J. M., & Watson, E. B. (2007). New thermodynamic models and revised calibrations for the Ti-in-zircon and Zr-in-rutile thermometers. *Contributions to Mineralogy and Petrology*, *154*(4), 429–437. https://doi.org/10.1007/s00410-007-0201-0

Ferré, E. C., Friedman, S. A., Martín-Hernández, F., Feinberg, J. M., Conder, J. A., & Ionov, D. A. (2013). The magnetism of mantle xenoliths and potential implications for sub-Moho magnetic sources. *Geophysical Research Letters*, *40*(1), 105–110. https://doi.org/10.1029/2012GL054100

Foley, S. F., Barth, M. G., Jenner, G. A., & Gunther, D. (2000). Partitioning of trace elements between rutile and silicate melts: Implications for subduction zones. *Geochimica et Cosmochimica Acta*, *64*(5), 933–938. https://doi.org/10.1016/j.gca.2004.11.015

Forshaw, J. B., Waters, D. J., Pattison, D. R. M., Palin, R. M., & Gopon, P. (2019). A comparison of observed and thermodynamically predicted phase equilibria and mineral compositions in mafic granulites. *Journal of Metamorphic Geology*, *37*(2), 153–179. https://doi.org/10.1111/jmg.12454

Frost, B. R., & Chacko, T. (1989). The granulite uncertainty principle: Limitations on thermobarometry in granulites. *The Journal of Geology*, *97*(4), 435–450. https://doi.org/10.1086/629321

Fuchs, S., Norden, B., & Commission, I. H. F. (2021). The global heat flow database: Release 2021. https://doi.org/10.5880/fidgeo.2021.014

Furlong, K. P., & Chapman, D. S. (2013). Heat flow, heat generation, and the thermal state of the lithosphere. *Annual Review of Earth and Planetary Sciences*, *41*(1), 385–410. https://doi.org/10.1146/annurev.earth.031208.100051

Garber, J. M., Maurya, S., Hernandez, J., Duncan, M. S., Zeng, L., Zhang, H. L., et al. (2018). Multidisciplinary constraints on the abundance of diamond and eclogite in the cratonic lithosphere. *Geochemistry, Geophysics, Geosystems*, *19*(7), 2062–2086. https://doi.org/10.1029/2018GC007534

Garber, J. M., Smye, A. J., Feineman, M. D., Kylander-Clark, A. R. C., & Matthews, S. (2020). Decoupling of zircon U–Pb and trace-element systematics driven by U diffusion in eclogite-facies zircon (Monviso meta-ophiolite, W. Alps). *Contributions to Mineralogy and Petrology*, *175*(6), 1–25. https://doi.org/10.1007/s00410-020-01692-2

Gard, M., & Hasterok, D. (2021). A global Curie depth model utilising the equivalent source magnetic dipole method. *Physics of the Earth and Planetary Interiors*, *313*(July 2020), 106672. https://doi.org/10.1016/j.pepi.2021.106672

Gladkochub, D. P., Donskaya, T. V., Ernst, R., Mazukabzov, A. M., Sklyarov, E. V., Pisarevsky, S. A., et al. (2012). Proterozoic basic magmatism of the Siberian Craton: Main stages and their geodynamic interpretation. *Geotectonics*, *46*(4), 273–284. https://doi.org/10.1134/S0016852112040024

Goes, S., Hasterok, D., Schutt, D. L., & Klöcking, M. (2020). Continental lithospheric temperatures: A review. *Physics of the Earth and Planetary Interiors*, *306*(May), 106509. https://doi.org/10.1016/j.pepi.2020.106509

Golovin, A. V., Sharygin, I. S., Kamenetsky, V. S., Korsakov, A. V., & Yaxley, G. M. (2018). Alkali-carbonate melts from the base of cratonic lithospheric mantle: Links to kimberlites. *Chemical Geology*, *483*(February), 261–274. https://doi.org/10.1016/j.chemgeo.2018.02.016

Golovin, A. V., Sharygin, I. S., Korsakov, A. V., Kamenetsky, V. S., & Abersteiner, A. (2020). Can primitive kimberlite melts be alkali-carbonate liquids: Composition of the melt snapshots preserved in deepest mantle xenoliths. *Journal of Raman Spectroscopy*, *51*(9), 1849–1867. https://doi.org/10.1002/jrs.5701

Goncharov, A. G., Ionov, D. A., Doucet, L. S., & Pokhilenko, L. N. (2012). Thermal state, oxygen fugacity and C-O-H fluid speciation in cratonic lithospheric mantle: New data on peridotite xenoliths from the Udachnaya kimberlite, Siberia. *Earth and Planetary Science Letters*, *357*(358), 99–110. https://doi.org/10.1016/j.epsl.2012.09.016

Green, E. C. R., White, R. W., Diener, J. F. A., Powell, R., Holland, T. J. B., & Palin, R. M. (2016). Activity-composition relations for the calculation of partial melting equilibria in metabasic rocks. *Journal of Metamorphic Geology*, *34*(9), 845–869. https://doi.org/10.1111/jmg.12211

Gruber, B., Chacko, T., Pearson, D. G., Currie, C., & Menzies, A. (2021). Heat production and Moho temperatures in cratonic crust: Evidence from lower crustal xenoliths from the slave craton. *Lithos*, *380–381*, 105889. https://doi.org/10.1016/j.lithos.2020.105889

Hacker, B. R., Gnos, E., Ratschbacher, L., Grove, M., McWilliams, M., Sobolev, S. V., et al. (2000). Hot and dry deep crustal xenoliths from Tibet. *Science*, *287*(5462), 2463–2466. https://doi.org/10.1126/science.287.5462.2463

Hacker, B. R., Kelemen, P. B., & Behn, M. D. (2015). Continental lower crust. *Annual Review of Earth and Planetary Sciences*, *43*(1), 167–205. https://doi.org/10.1146/annurev-earth-050212-124117

Harley, S. L. (1989). The origins of granulites: A metamorphic perspective. *Geological Magazine*, *126*(3), 215–247. https://doi.org/10.1017/S0016756800022330

Hasterok, D., & Chapman, D. S. (2011). Heat production and geotherms for the continental lithosphere. *Earth and Planetary Science Letters*, *307*(1–2), 59–70. https://doi.org/10.1016/j.epsl.2011.04.034

Hiess, J., Condon, D. J., McLean, N., & Noble, S. R. (2012). $^{238}U/^{235}U$ systematics in terrestrial uranium-bearing minerals. *Science*, *335*(6076), 1610–1614. https://doi.org/10.1126/science.1215507

Holder, R. M., Hacker, B. R., Seward, G. G. E., & Kylander-Clark, A. R. C. (2019). Interpreting titanite U–Pb dates and Zr thermobarometry in high-grade rocks: Empirical constraints on elemental diffusivities of Pb, Al, Fe, Zr, Nb, and Ce. *Contributions to Mineralogy and Petrology*, *174*(5), 42. https://doi.org/10.1007/s00410-019-1578-2

Holland, T., & Blundy, J. (1994). Non-ideal interactions in calcic amphiboles and their bearing on amphibole-plagioclase thermometry. *Contributions to Mineralogy and Petrology*, *116*(4), 433–447. https://doi.org/10.1007/BF00310910

Holland, T. J. B. (1980). The reaction albite = jadeite + quartz determined experimentally in the range 600–1200°C. *American Mineralogist*, *65*, 129–134. Retrieved from http://ammin.geoscienceworld.org/content/65/1-2/129.short

Holland, T. J. B., & Powell, R. (2011). An improved and extended internally consistent thermodynamic dataset for phases of petrological interest, involving a new equation of state for solids. *Journal of Metamorphic Geology*, *29*(3), 333–383. https://doi.org/10.1111/j.1525-1314.2010.00923.x

Horstwood, M. S. A., Košler, J., Gehrels, G., Jackson, S. E., McLean, N. M., Paton, C., et al. (2016). Community-derived standards for LA-ICP-MS U-(Th-)Pb geochronology – Uncertainty propagation, age interpretation and data reporting. *Geostandards and Geoanalytical Research*, *40*(3), 311–332. https://doi.org/10.1111/j.1751-908X.2016.00379.x

Ionov, D. A., Doucet, L. S., & Ashchepkov, I. V. (2010). Composition of the lithospheric mantle in the Siberian craton: New constraints from fresh peridotites in the Udachnaya-East Kimberlite. *Journal of Petrology*, *51*(11), 2177–2210. https://doi.org/10.1093/petrology/egq053

Ionov, D. A., Doucet, L. S., Carlson, R. W., Golovin, A. V., & Korsakov, A. V. (2015). Post-Archean formation of the lithospheric mantle in the central Siberian craton: Re–Os and PGE study of peridotite xenoliths from the Udachnaya kimberlite. *Geochimica et Cosmochimica Acta*, *165*, 466–483. https://doi.org/10.1016/j.gca.2015.06.035

15252027, 2022, 10, Downloaded from https://agupubs.onlinelibrary.wiley.com/doi/10.1029/2022GC010497 by Cochrane France, Wiley Online Library on [21/10/2022]. See the Terms and Conditions (https://onlinelibrary.wiley.com/terms-and-conditions) on Wiley Online Library for rules of use; OA articles are governed by the applicable Creative Commons License

Ionov, D. A., Liu, Z., Li, J., Golovin, A. V., Korsakov, A. V., & Xu, Y. (2020). The age and origin of cratonic lithospheric mantle: Archean dunites vs. Paleoproterozoic harzburgites from the Udachnaya kimberlite, Siberian craton. *Geochimica et Cosmochimica Acta*, *281*, 67–90. https://doi.org/10.1016/j.gca.2020.05.009

Jaupart, C., & Mareschal, J. (2007). Heat flow and thermal structure of the lithosphere. In *Volume 6: Crust and lithosphere dynamics* (Vol. 6, pp. 217–251). Elsevier. https://doi.org/10.1016/B978-044452748-6/00104-8

Jaupart, C., & Mareschal, J.-C. (2014). Constraints on Crustal heat production from heat flow data. In *Treatise on geochemistry* (2nd ed., Vol. 4, pp. 53–73). Elsevier. https://doi.org/10.1016/B978-0-08-095975-7.00302-8

Jaupart, C., Mareschal, J.-C., & Iarotsky, L. (2016). Radiogenic heat production in the continental crust. *Lithos*, *262*(August), 398–427. https://doi.org/10.1016/j.lithos.2016.07.017

Jin, T., Wang, Q., Shatsky, V., & Liao, Y. (2021). Water content and deformation of the lower crust beneath the Siberian Craton: Evidence from granulite xenoliths. *The Journal of Geology*, *129*(5), 475–498. https://doi.org/10.1086/716514

Jollands, M. C., Hanger, B. J., Yaxley, G. M., Hermann, J., & Kilburn, M. R. (2018). Timescales between mantle metasomatism and kimberlite ascent indicated by diffusion profiles in garnet crystals from peridotite xenoliths. *Earth and Planetary Science Letters*, *481*, 143–153. https://doi.org/10.1016/j.epsl.2017.10.021

Jones, A. P., Smith, J. V., Dawson, J. B., & Hansen, E. C. (1983). Metamorphism, partial melting, and K-metasomatism of garnet-scapolite-kyanite granulite xenoliths from Lashaine, Tanzania. *The Journal of Geology*, *91*(2), 143–165. https://doi.org/10.1086/628753

Kamenetsky, V. S., Kamenetsky, M. B., Sharygin, V. V., Faure, K., & Golovin, A. V. (2007). Chloride and carbonate immiscible liquids at the closure of the kimberlite magma evolution (Udachnaya-East kimberlite, Siberia). *Chemical Geology*, *237*(3–4), 384–400. https://doi.org/10.1016/j.chemgeo.2006.07.010

Kinny, P. D., Griffin, B. J., & Brakhfogel, F. F. (1995). Shrimp U/Pb ages of perovskite and zircon from Yakutian kimberlites. In *International Kimberlite Conference Extended Abstracts 1995* (Vol. 8, pp. 55). University of Alberta Library. https://doi.org/10.29173/ikc1860

Kitayama, Y., Thomassot, E., Galy, A., Golovin, A., Korsakov, A., d'Eyrames, E., et al. (2017). Co-magmatic sulfides and sulfates in the Udachnaya-East pipe (Siberia): A record of the redox state and isotopic composition of sulfur in kimberlites and their mantle sources. *Chemical Geology*, *455*, 315–330. https://doi.org/10.1016/j.chemgeo.2016.10.037

Kitayama, Y., Thomassot, E., Galy, A., Korsakov, A., Golovin, A., & D'Eyrames, E. (2021). Geochemical evidence for carbon and chlorine enrichments in the mantle source of kimberlites (Udachnaya pipe, Siberian craton). *Geochimica et Cosmochimica Acta*, *315*, 295–316. https://doi.org/10.1016/j.gca.2021.09.021

Klemme, S., Prowatke, S., Hametner, K., & Günther, D. (2005). Partitioning of trace elements between rutile and silicate melts: Implications for subduction zones. *Geochimica et Cosmochimica Acta*, *69*(9), 2361–2371. https://doi.org/10.1016/j.gca.2004.11.015

Kohn, M. J., Penniston-Dorland, S. C., & Ferreira, J. C. S. (2016). Implications of near-rim compositional zoning in rutile for geothermometry, geospeedometry, and trace element equilibration. *Contributions to Mineralogy and Petrology*, *171*(10), 78. https://doi.org/10.1007/s00410-016-1285-1

Koreshkova, M., Downes, H., Nikitina, L., Vladykin, N., Larionov, A., & Sergeev, S. (2009). Trace element and age characteristics of zircons in granulite xenoliths from the Udachnaya kimberlite pipe, Siberia. *Precambrian Research*, *168*(3–4), 197–212. https://doi.org/10.1016/j.precamres.2008.09.007

Koreshkova, M. Y., Downes, H., Levsky, L. K., & Vladykin, N. V. (2011). Petrology and geochemistry of granulite xenoliths from Udachnaya and Komsomolskaya kimberlite pipes, Siberia. *Journal of Petrology*, *52*(10), 1857–1885. https://doi.org/10.1093/petrology/egr033

Kostrovitsky, S. I., Skuzovatov, S. Y., Yakovlev, D. A., Sun, J., Nasdala, L., & Wu, F.-Y. (2016). Age of the Siberian craton crust beneath the northern kimberlite fields: Insights to the craton evolution. *Gondwana Research*, *39*, 365–385. https://doi.org/10.1016/j.gr.2016.01.008

Kylander-Clark, A. R. C. (2017). Petrochronology by laser-ablation inductively coupled plasma mass spectrometry. *Reviews in Mineralogy and Geochemistry*, *83*(1), 183–198. https://doi.org/10.2138/rmg.2017.83.6

Kylander-Clark, A. R. C., Hacker, B. R., & Cottle, J. M. (2013). Laser-ablation split-stream ICP petrochronology. *Chemical Geology*, *345*, 99–112. https://doi.org/10.1016/j.chemgeo.2013.02.019

Liu, Z., Ionov, D. A., Nimis, P., Xu, Y., He, P., & Golovin, A. V. (2022). Thermal and compositional anomalies in a detailed xenolith-based lithospheric mantle profile of the Siberian craton and the origin of seismic midlithosphere discontinuities. *Geology*, *50*(8), 891–896. https://doi.org/10.1130/G49947.1

Mackey, K. G., Fujita, K., & Ruff, L. J. (1998). Crustal thickness of northeast Russia. *Tectonophysics*, *284*(3–4), 283–297. https://doi.org/10.1016/S0040-1951(97)00180-7

Marschall, H. R., Dohmen, R., & Ludwig, T. (2013). Diffusion-induced fractionation of niobium and tantalum during continental crust formation. *Earth and Planetary Science Letters*, *375*, 361–371. https://doi.org/10.1016/j.epsl.2013.05.055

McIntyre, T., Kublik, K., Currie, C., & Pearson, D. G. (2021). Heat generation in cratonic mantle roots—New trace element constraints from mantle xenoliths and Implications for cratonic geotherms. *Geochemistry, Geophysics, Geosystems*, *22*(9), 1–25. https://doi.org/10.1029/2021GC009691

Molina, J. F., Moreno, J. A., Castro, A., Rodríguez, C., & Fershtater, G. B. (2015). Calcic amphibole thermobarometry in metamorphic and igneous rocks: New calibrations based on plagioclase/amphibole Al-Si partitioning and amphibole/liquid Mg partitioning. *Lithos*, *232*, 286–305. https://doi.org/10.1016/j.lithos.2015.06.027

Moyen, J.-F., Paquette, J.-L., Ionov, D. A., Gannoun, A., Korsakov, A. V., Golovin, A. V., & Moine, B. N. (2017). Paleoproterozoic rejuvenation and replacement of Archaean lithosphere: Evidence from zircon U–Pb dating and Hf isotopes in crustal xenoliths at Udachnaya, Siberian craton. *Earth and Planetary Science Letters*, *457*, 149–159. https://doi.org/10.1016/j.epsl.2016.09.046

Newton, R. C., & Perkins, D. (1982). Thermodynamic calibration of geobarometers based on the assemblages garnet-plagioclase-orthopyroxene (clinopyroxene)-quartz. *American Mineralogist*, *67*(3–4), 203–222.

Nicolaysen, L. O., Hart, R. J., & Gale, N. H. (1981). The Vredefort radioelement profile extended to supracrustal strata at Carletonville, with implications for continental heat flow. *Journal of Geophysical Research*, *86*(B11), 10653–10661. https://doi.org/10.1029/JB086iB11p10653

Nimis, P., Goncharov, A., Ionov, D. A., & McCammon, C. (2015). Fe^{3+} partitioning systematics between orthopyroxene and garnet in mantle peridotite xenoliths and implications for thermobarometry of oxidized and reduced mantle rocks. *Contributions to Mineralogy and Petrology*, *169*(1), 6. https://doi.org/10.1007/s00410-014-1101-8

O'Brien, P. J., & Rotzler, J. (2003). High-pressure granulites: Formation, recovery of peak conditions and implications for tectonics. *Journal of Metamorphic Geology*, *21*(1), 3–20. https://doi.org/10.1046/j.1525-1314.2003.00420.x

O'Sullivan, G. J., Thakurdin, Y., Bolhar, R., Horváth, P., Hoare, B. C., & Collerson, K. D. (2021). The Great Falls tectonic zone after the assembly of Laurentia: Evidence for long-term tectonic stability from xenolith apatite. *Lithos*, *384–385*, 105977. https://doi.org/10.1016/j.lithos.2021.105977

Palin, R. M., White, R. W., Green, E. C. R., Diener, J. F. A., Powell, R., & Holland, T. J. B. (2016). High-grade metamorphism and partial melting of basic and intermediate rocks. *Journal of Metamorphic Geology*, *34*(9), 871–892. https://doi.org/10.1111/jmg.12212

15252027, 2022, 10, Downloaded from https://agupubs.onlinelibrary.wiley.com/doi/10.1029/2022GC010497 by Cochrane France, Wiley Online Library on [21/10/2022]. See the Terms and Conditions (https://onlinelibrary.wiley.com/terms-and-conditions) on Wiley Online Library for rules of use; OA articles are governed by the applicable Creative Commons License

Paquette, J. L., Ionov, D. A., Agashev, A. M., Gannoun, A., & Nikolenko, E. I. (2017). Age, provenance and Precambrian evolution of the Anabar shield from U-Pb and Lu-Hf isotope data on detrital zircons, and the history of the northern and central Siberian craton. *Precambrian Research*, *301*(September), 134–144. https://doi.org/10.1016/j.precamres.2017.09.008

Pattison, D. R. M. (2003). Petrogenetic significance of orthopyroxene-free garnet + clinopyroxene + plagioclase ± quartz-bearing metabasites with respect to the amphibolite and granulite facies. *Journal of Metamorphic Geology*, *21*(1), 21–34. https://doi.org/10.1046/j.1525-1314.2003.00415.x

Pattison, D. R. M., & Bégin, N. J. (1994). Zoning patterns in orthopyroxene and garnet in granulites: Implications for geothermometry. *Journal of Metamorphic Geology*, *12*(4), 387–410. https://doi.org/10.1111/j.1525-1314.1994.tb00031.x

Pearson, D. G., Shirey, S. B., Carlson, R. W., Boyd, F. R., Pokhilenko, N. P., & Shimizu, N. (1995). Re-Os, Sm-Nd, and Rb-Sr isotope evidence for thick Archaean lithospheric mantle beneath the Siberian craton modified by multistage metasomatism. *Geochimica et Cosmochimica Acta*, *59*(5), 959–977. https://doi.org/10.1016/0016-7037(95)00014-3

Powell, R., Holland, T., & Worley, B. (1998). Calculating phase diagrams involving solid solutions via non-linear equations, with examples using THERMOCALC. *Journal of Metamorphic Geology*, *16*(4), 577–588. https://doi.org/10.1111/j.1525-1314.1998.00157.x

Priyatkina, N., Khudoley, A. K., Collins, W. J., Kuznetsov, N. B., & Huang, H. Q. (2016). Detrital zircon record of Meso- and Neoproterozoic sedimentary basins in northern part of the Siberian Craton: Characterizing buried crust of the basement. *Precambrian Research*, *285*, 21–38. https://doi.org/10.1016/j.precamres.2016.09.003

Rosen, O. M. (1989). Two geochemically different types of Precambrian crust in the Anabar shield, North Siberia. *Precambrian Research*, *45*(1–3), 129–142. https://doi.org/10.1016/0301-9268(89)90035-1

Rosen, O. M. (2002). Siberian craton – A fragment of a Paleoproterozoic supercontinent. *Russian Journal of Earth Sciences*, *4*(2), 103–119. https://doi.org/10.2205/2002ES000090

Rosen, O. M., Levskii, L. K., Zhuravlev, D. Z., Rotman, A. Y., Spetsius, Z. V., Makeev, A. F., et al. (2006). Paleoproterozoic accretion in the Northeast Siberian craton: Isotopic dating of the Anabar collision system. *Stratigraphy and Geological Correlation*, *14*(6), 581–601. https://doi.org/10.1134/S0869593806060013

Rudnick, R. L., & Fountain, D. M. (1995). Nature and composition of the continental crust: A lower crustal perspective. *Reviews of Geophysics*, *33*(3), 267. https://doi.org/10.1029/95RG01302

Rudnick, R. L., & Gao, S. (2014). Composition of the continental crust. In *Treatise on geochemistry* (2nd ed., Vol. 4, pp. 1–51). Elsevier. https://doi.org/10.1016/B978-0-08-095975-7.00301-6

Rudnick, R. L., McDonough, W. F., & O'Connell, R. J. (1998). Thermal structure, thickness and composition of continental lithosphere. *Chemical Geology*, *145*(3–4), 395–411. https://doi.org/10.1016/S0009-2541(97)00151-4

Rudnick, R. L. R., & Nyblade, A. (1999). The thickness and heat production of Archean lithosphere: Constraints from xenolith thermobarometry and surface heat flow. *Mantle Petrology: Field Observations and High Pressure Experimentation (a Tribute to Francis R. (Joe) Boyd)*, *6*(6), 3–12.

Sandiford, M., & McLaren, S. (2002). Tectonic feedback and the ordering of heat producing elements within the continental lithosphere. *Earth and Planetary Science Letters*, *204*(1–2), 133–150. https://doi.org/10.1016/S0012-821X(02)00958-5

Sandiford, M., Mclaren, S., & Neumann, N. (2002). Long-term thermal consequences of the redistribution of heat-producing elements associated with large-scale granitic complexes. *Journal of Metamorphic Geology*, *20*(1), 87–98. https://doi.org/10.1046/j.0263-4929.2001.00359.x

Sasaki, J., Peterson, N. L., & Hoshino, K. (1985). Tracer impurity diffusion in single-crystal rutile (TiO_2−x). *Journal of Physics and Chemistry of Solids*, *46*(11), 1267–1283. https://doi.org/10.1016/0022-3697(85)90129-5

Schmitz, M. D., & Bowring, S. A. (2003). Constraints on the thermal evolution of continental lithosphere from U-Pb accessory mineral thermochronometry of lower crustal xenoliths, southern Africa. *Contributions to Mineralogy and Petrology*, *144*(5), 592–618. https://doi.org/10.1007/s00410-002-0419-9

Semprich, J., & Simon, N. S. C. (2014). Inhibited eclogitization and consequences for geophysical rock properties and delamination models: Constraints from cratonic lower crustal xenoliths. *Gondwana Research*, *25*(2), 668–684. https://doi.org/10.1016/j.gr.2012.08.018

Shatsky, V., Ragozin, A., Zedgenizov, D., & Mityukhin, S. (2008). Evidence for multistage evolution in a xenolith of diamond-bearing eclogite from the Udachnaya kimberlite pipe. *Lithos*, *105*(3–4), 289–300. https://doi.org/10.1016/j.lithos.2008.04.008

Shatsky, V. S., Malkovets, V. G., Belousova, E. A., Tretiakova, I. G., Griffin, W. L., Ragozin, A. L., et al. (2016). Tectonothermal evolution of the continental crust beneath the Yakutian diamondiferous province (Siberian craton): U–Pb and Hf isotopic evidence on zircons from crustal xenoliths of kimberlite pipes. *Precambrian Research*, *282*, 1–20. https://doi.org/10.1016/j.precamres.2016.06.022

Shatsky, V. S., Wang, Q., Skuzovatov, S. Y., & Ragozin, A. L. (2019). The crust-mantle evolution of the Anabar tectonic province in the Siberian Craton: Coupled or decoupled? *Precambrian Research*, *332*(July), 105388. https://doi.org/10.1016/j.precamres.2019.105388

Smelov, A. P., Kotov, A. B., Sal'nikova, E. B., Kovach, V. P., Beryozkin, V. I., Kravchenko, A. A., et al. (2012). Age and duration of the formation of the Billyakh tectonic melange zone, Anabar Shield. *Petrology*, *20*(3), 286–300. https://doi.org/10.1134/S0869591112030058

Smit, M. A., Waight, T. E., & Nielsen, T. F. D. (2016). Millennia of magmatism recorded in crustal xenoliths from alkaline provinces in Southwest Greenland. *Earth and Planetary Science Letters*, *451*, 241–250. https://doi.org/10.1016/j.epsl.2016.06.047

Smye, A. J., & Stockli, D. F. (2014). Rutile U–Pb age depth profiling: A continuous record of lithospheric thermal evolution. *Earth and Planetary Science Letters*, *408*, 171–182. https://doi.org/10.1016/j.epsl.2014.10.013

Smye, A. J., Marsh, J. H., Vermeesch, P., Garber, J. M., & Stockli, D. F. (2018). Applications and limitations of U-Pb thermochronology to middle and lower crustal thermal histories. *Chemical Geology*, *494*(July), 1–18. https://doi.org/10.1016/j.chemgeo.2018.07.003

Spera, F. J. (1984). Carbon dioxide in petrogenesis III: Role of volatiles in the ascent of alkaline magma with special reference to xenolith-bearing mafic lavas. *Contributions to Mineralogy and Petrology*, *88*(3), 217–232. https://doi.org/10.1007/BF00380167

Stacey, J. S., & Kramers, J. D. (1975). Approximation of terrestrial lead isotope evolution by a two-stage model. *Earth and Planetary Science Letters*, *26*(2), 207–221. https://doi.org/10.1016/0012-821X(75)90088-6

Stearns, M. A., Cottle, J. M., Hacker, B. R., & Kylander-Clark, A. R. C. (2016). Extracting thermal histories from the near-rim zoning in titanite using coupled U-Pb and trace-element depth profiles by single-shot laser-ablation split stream (SS-LASS) ICP-MS. *Chemical Geology*, *422*, 13–24. https://doi.org/10.1016/j.chemgeo.2015.12.011

Sun, J., Liu, C.-Z., Tappe, S., Kostrovitsky, S. I., Wu, F.-Y., Yakovlev, D., et al. (2014). Repeated kimberlite magmatism beneath Yakutia and its relationship to Siberian flood volcanism: Insights from in situ U–Pb and Sr–Nd perovskite isotope analysis. *Earth and Planetary Science Letters*, *404*, 283–295. https://doi.org/10.1016/j.epsl.2014.07.039

Tomkins, H. S., Powell, R., & Ellis, D. J. (2007). The pressure dependence of the zirconium-in-rutile thermometer. *Journal of Metamorphic Geology*, *25*(6), 703–713. https://doi.org/10.1111/j.1525-1314.2007.00724.x

Vermeesch, P. (2018). IsoplotR: A free and open toolbox for geochronology. *Geoscience Frontiers*, *9*(5), 1479–1493. https://doi.org/10.1016/j.gsf.2018.04.001

15252027, 2022, 10, Downloaded from https://agupubs.onlinelibrary.wiley.com/doi/10.1029/2022GC010497 by Cochrane France, Wiley Online Library on [21/10/2022]. See the Terms and Conditions (https://onlinelibrary.wiley.com/terms-and-conditions) on Wiley Online Library for rules of use; OA articles are governed by the applicable Creative Commons License

Whitney, D. L., & Evans, B. W. (2010). Abbreviations for names of rock-forming minerals. *American Mineralogist*, *95*(1), 185–187. https://doi.org/10.2138/am.2010.3371

References From the Supporting Information

Apen, F. E., Wall, C. J., Cottle, J. M., Schmitz, M. D., Kylander-Clark, A. R. C., & Seward, G. G. E. (2022). Apatites for destruction: Reference apatites from Morocco and Brazil for U-Pb petrochronology and Nd and Sr isotope geochemistry. *Chemical Geology*, *590*(December 2021), 120689. https://doi.org/10.1016/j.chemgeo.2021.120689

Ewing, T. A., Rubatto, D., Beltrando, M., & Hermann, J. (2015). Constraints on the thermal evolution of the Adriatic margin during Jurassic continental break-up: U–Pb dating of rutile from the Ivrea–Verbano zone, Italy. *Contributions to Mineralogy and Petrology*, *169*(4), 44. https://doi.org/10.1007/s00410-015-1135-6

Fuhrman, M. L., & Lindsley, D. H. (1988). Ternary-feldspar modeling and thermometry. *American Mineralogist*, *73*, 201–215.

Green, E., Holland, T., & Powell, R. (2007). An order-disorder model for omphacitic pyroxenes in the system jadeite-diopside-hedenbergite-acmite, with applications to eclogitic rocks. *American Mineralogist*, *92*(7), 1181–1189. https://doi.org/10.2138/am.2007.2401

Jackson, S. E., Pearson, N. J., Griffin, W. L., & Belousova, E. A. (2004). The application of laser ablation-inductively coupled plasma-mass spectrometry to in situ U–Pb zircon geochronology. *Chemical Geology*, *211*(1–2), 47–69. https://doi.org/10.1016/j.chemgeo.2004.06.017

Kylander-Clark, A. R. C., Hacker, B. R., & Mattinson, J. M. (2008). Slow exhumation of UHP terranes: Titanite and rutile ages of the Western Gneiss Region, Norway. *Earth and Planetary Science Letters*, *272*(3–4), 531–540. https://doi.org/10.1016/j.epsl.2008.05.019

Liu, Y., Hu, Z., Gao, S., Günther, D., Xu, J., Gao, C., & Chen, H. (2008). In situ analysis of major and trace elements of anhydrous minerals by LA-ICP-MS without applying an internal standard. *Chemical Geology*, *257*(1–2), 34–43. https://doi.org/10.1016/j.chemgeo.2008.08.004

Luvizotto, G. L., Zack, T., Meyer, H. P., Ludwig, T., Triebold, S., Kronz, A., et al. (2009). Rutile crystals as potential trace element and isotope mineral standards for microanalysis. *Chemical Geology*, *261*(3–4), 346–369. https://doi.org/10.1016/j.chemgeo.2008.04.012

McKinney, S. T., Cottle, J. M., & Lederer, G. W. (2015). Evaluating rare Earth element (REE) mineralization mechanisms in Proterozoic gneiss, Music Valley, California. *The Geological Society of America Bulletin*, *127*(7–8), B31165.1. https://doi.org/10.1130/B31165.1

Paton, C., Hellstrom, J., Paul, B., Woodhead, J., & Hergt, J. (2011). Iolite: Freeware for the visualisation and processing of mass spectrometric data. *Journal of Analytical Atomic Spectrometry*, *26*(12), 2508. https://doi.org/10.1039/c1ja10172b

Schoene, B., & Bowring, S. A. (2006). U–Pb systematics of the McClure mountain syenite: Thermochronological constraints on the age of the $^{40}Ar/^{39}Ar$ standard MMhb. *Contributions to Mineralogy and Petrology*, *151*(5), 615–630. https://doi.org/10.1007/s00410-006-0077-4

Sláma, J., Košler, J., Condon, D. J., Crowley, J. L., Gerdes, A., Hanchar, J. M., et al. (2008). Plešovice zircon – A new natural reference material for U-Pb and Hf isotopic microanalysis. *Chemical Geology*, *249*(1–2), 1–35. https://doi.org/10.1016/j.chemgeo.2007.11.005

Thompson, J., Meffre, S., Maas, R., Kamenetsky, V., Kamenetsky, M., Goemann, K., et al. (2016). Matrix effects in Pb/U measurements during LA-ICP-MS analysis of the mineral apatite. *Journal of Analytical Atomic Spectrometry*, *31*(6), 1206–1215. https://doi.org/10.1039/C6JA00048G

White, R. W., Powell, R., Holland, T. J. B., Johnson, T. E., & Green, E. C. R. (2014). New mineral activity-composition relations for thermodynamic calculations in metapelitic systems. *Journal of Metamorphic Geology*, *32*(3), 261–286. https://doi.org/10.1111/jmg.12071

White, R. W., Powell, R., Holland, T. J. B., & Worley, B. A. (2000). The effect of TiO_2 and Fe_2O_3 on metapelitic assemblages at greenschist and amphibolite facies conditions: Mineral equilibria calculations in the system K_2O-FeO-MgO-Al_2O_3-SiO_2-H_2O-TiO_2-Fe_2O_3. *Journal of Metamorphic Geology*, *18*(5), 497–511. https://doi.org/10.1046/j.1525-1314.2000.00269.x

15252027, 2022, 10, Downloaded from https://agupubs.onlinelibrary.wiley.com/doi/10.1029/2022GC010497 by Cochrane France, Wiley Online Library on [21/10/2022]. See the Terms and Conditions (https://onlinelibrary.wiley.com/terms-and-conditions) on Wiley Online Library for rules of use; OA articles are governed by the applicable Creative Commons License